Nanoscale

ROYAL SOCIETY OF CHEMISTRY

MINIREVIEW

View Article Online
View Journal | View Issue

Cite this: *Nanoscale*, 2024, **16**, 6915

Gallium-based liquid metals as reaction media for nanomaterials synthesis

Ming Wang and Yiliang Lin *

Gallium-based liquid metals (LMs) and their alloys have gained prominence in the realm of flexible and stretchable electronics. Recent advances have expanded the interest to explore the electron-rich core and interface of LMs to synthesize various nanomaterials, where Ga-based LMs serve as versatile reaction media. In this paper, we delve into the latest developments within this burgeoning field. Our discussion begins by elucidating the unique attributes of LMs that render them suitable as reaction media, including their high metal solubility, low standard reduction potential, self-limiting oxidation and ultra-smooth and "layer" surface. We then provide a comprehensive categorized summary of utilizing these features to fabricate a variety of nanomaterials, including pure metallic materials (metal alloys, metal crystals, porous metals, high-entropy alloys and metallic single atoms), metal–inorganic compounds (2D metal oxides, 2D metallic inorganic compounds and 2D graphitic materials), as well as metal–organic composites (metal–organic frameworks). This paper concludes by discussing the current challenges in this field and exploring potential future directions. The versatility and unique properties of Ga-based LMs are poised to play a pivotal role in the future of nanomaterial science, paving the way for more efficient, sustainable, and innovative technological solutions.

Received 23rd December 2023,
Accepted 29th February 2024

DOI: 10.1039/d3nr06566a

rsc.li/nanoscale

1 Introduction

Liquid metals (LMs) with low melting points are increasingly garnering interest in several critical fields, owing to their unique combination of room temperature fluidity, metallic conductivity and superior thermal conductivity. Among them, mercury (Hg), cesium (Cs) and rubidium (Rb) are being progressively eliminated from use due to their high chemical instability, radioactivity or toxicity.[1,2] Gallium (Ga) is known for its non-toxicity and has a melting point of 29.7 °C. Ga uniquely exhibits both metallic and covalent bonding, allowing it to remain a liquid over a broad temperature range (up to approximately 2000 °C), while maintaining a low vapor pressure.[2,3] Additionally, it exhibits remarkable stability in air and water.[3] Apart from Ga, Ga-based LMs can be derived from binary or ternary mixtures of other post-transition metals (indium (In), tin (Sn), aluminum (Al), zinc (Zn), Hg, *etc.*).[4,5] This approach allows for adjusting the melting point range from 13.2 to 27.0 °C, offering versatile applications in various fields.

These LMs exhibit properties characteristic of both metallic and covalent bonds, marked by an abundance of free electrons and disordered ions.[6,7] Consequently, various metal elements can dissolve, precipitate, diffuse mutually and form intermetallic compounds within the LM matrix, making them ideal reaction media for materials synthesis.[8–11] Significantly, Ga features a low standard reduction potential ($E_0[Ga^{3+}/Ga^0]$ = −0.529 V *vs.* the standard hydrogen electrode (SHE)), endowing it with a highly active surface for catalytic or reduction interface reactions.[12,13] More interestingly, LMs spontaneously form an ultra-thin oxide layer when exposed to air.[14,15] This oxide skin, with weak adhesion to the nonpolar surface of the

Department of Chemical and Biomolecular Engineering, National University of Singapore, Engineering Drive 4, 117585, Singapore. E-mail: y.lin@nus.edu.sg

Yiliang Lin

Dr Yiliang Lin currently holds the position of Assistant Professor in the Department of Chemical and Biomolecular Engineering at the National University of Singapore. He completed his Ph.D. in Chemical Engineering at North Carolina State University in 2018, followed by a postdoctoral research stint at the University of Chicago. In November 2023, Dr Lin joined the National University of Singapore and founded his research group. His team is dedicated to the innovative design and development of soft materials and living materials, with a focus on applications in human–machine interfaces, biomedical therapies, and sustainability initiatives.

flowing metallic matrix, is easily transferable to any desired substrate.[16,17] However, upon the removal of the oxide skin, LMs can provide atomically smooth interfaces, making them suitable as soft and ultra-smooth templates for low temperature deposition and 2D material growth.[18,19]

In this review, we focus on the latest developments in the synthesis of exciting nanomaterials utilizing Ga-based LMs as reaction media. We begin with a concise overview of the distinctive characteristics pertinent to Ga-based LM reactors, including their high metal solubility, low standard reduction potential, self-limiting oxidation as well as ultra-smooth and "layer" surface. Consequently, we highlight recent application examples and fabrication strategies in the synthesis of diverse materials, such as metal alloys, metal crystals, porous metals, high-entropy alloys, metallic single atoms, 2D metal oxides, 2D metallic inorganic compounds, 2D graphitic materials and metal–organic frameworks, as illustrated in Fig. 1. Lastly, we discuss the existing challenges and explore potential opportunities in the realm of LM reactors, aiming to shed light on their future prospects and applications.

2 Attributes of Ga-based liquid metals

2.1 High metal solubility in LMs

Distinct from conventional liquid solvents, Ga-based LMs stand out as dense and highly interactive liquid solvents.[9] Their broad melting range, reductive fluid environment and electron-rich composition, and the abundance of vacancies in their bulk allow them to solvate or disperse a wide range of metallic elements (Fig. 2a). This assortment includes various post-transition metals, transition metals, lanthanides, alkali metals and rare-earth elements, and even some semimetals like silicon,[20] all maintained in a neutral state to form eutectic alloys or composites.[2,4,21,22] Notably, these alloys or composites can serve as unique stand-alone droplet microreactors, promoting liquid–solid interfacial interactions within the droplet. This facilitates the formation of ordered crystalline phases of intermetallic compounds even below the melting temperature of the individual elements involved.[6,23,24] Prominent examples include eutectic alloys of Ga and In (EGaIn) and galinstan (eutectic alloys of Ga, In and Sn) with melting points of 15.4 °C and 13.2 °C, respectively (Table 1).[18] The high metal solubility of Ga-based LMs renders them valuable in various scientific applications, particularly in the synthesis of new materials and compounds.

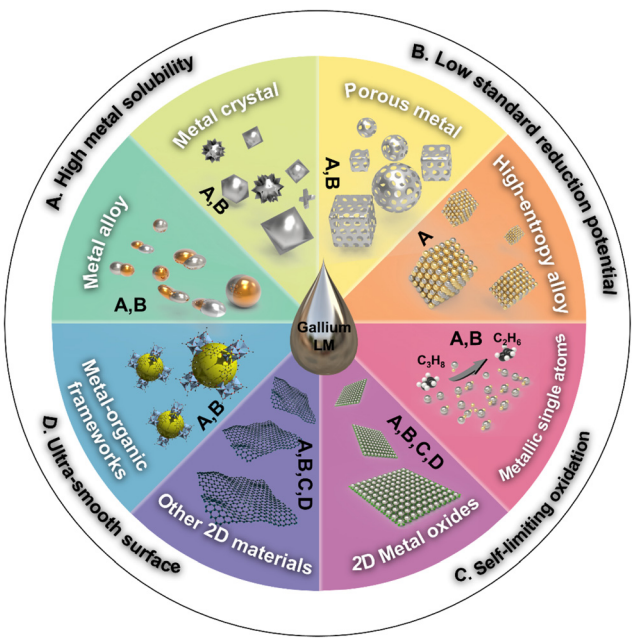

Fig. 1 Attributes of Ga-based LMs and the corresponding nanomaterials synthesis. The key properties of the liquid Ga are labeled as A, B, C and D to convey the relationship between the synthesized nanomaterials and the utilized properties of Ga-based LMs.

2.2 Low standard reduction potential

In the electrochemical series, Ga is in such a position (E_0Ga/Ga^{3+} = −0.549) that it can theoretically reduce metal ions with a higher standard electrode potential than itself to their metallic form (Fig. 2b).[24–27] This characteristic facilitates surface modification of LMs through a galvanic replacement reaction (GRR), as illustrated in Fig. 2c. The general principle of this reaction is summarized as the following equation,

$$\mathrm{Ga} + \frac{3}{n}\mathrm{Me}^{n+} \rightleftharpoons \mathrm{Ga}^{3+} + \frac{3}{n}\mathrm{Me}$$

where the standard electrode potential value of the element 'Me' (metals) should be greater than that of Ga, as highlighted by the elements marked in red in the periodic table (Fig. 2b).[28]

In addition to the reduced-state metallic materials, non-metallic structures such as reduced state graphene oxide (rGO), can also be obtained on LM surfaces *via* the electrochemical reactions.[29] These surface modifications not only improve stability under harsh conditions, but also modulate fundamental properties such as catalytic activity.

2.3 Oxide skin on the LM surface

Upon exposure to oxygen (>1 part per million), Ga rapidly forms a self-limiting oxide skin,[30] and the self-limiting oxidation process can be explained by the Cabrera–Mott metal oxidation model (Fig. 3a).[31] The thickness of the final oxide layer, typically just a few nanometers, has been confirmed through various methods, such as X-ray reflectivity analysis,[32] transmission electron microscopy (TEM) (Fig. 3b)[33] and angle-resolved X-ray photoelectron spectroscopy (XPS).[34] This atomically thin interfacial oxide is regarded as a naturally occurring 2D material.[35]

The oxide skin significantly alters the physical and chemical properties of Ga-based LMs, affecting their surface chemistry, wetting behavior and rheological properties.[36] Furthermore, the oxide skin also enhances the adhesion of the metal substrate, allowing it to firmly adhere (or 'wet') more efficiently with many substrates, particularly like glass, quartz,

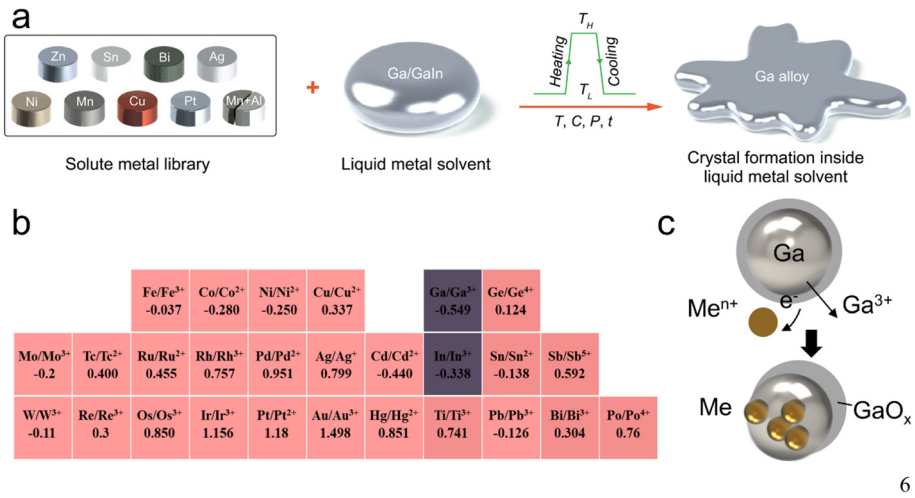

Fig. 2 Ga-based LMs have high metal solubility and a low standard reduction potential. (a) The procedures for forming metal alloys or growing metal crystals in liquid Ga solvents. Reprinted with permission.[9] Copyright (2022), American Association for the Advancement of Science. (b) Standard reduction potentials for selected elements in the periodic table; elements marked in red could be reduced by Ga. (c) Sketch of the GRR scheme based on liquid Ga. Metal salt ions (Me^{n+}) pass through the pores in the Ga oxide shell and are reduced to their metal form by Ga.

Table 1 The composition and melting point (<60 °C) of commonly used Ga-based LMs

Alloyed elements	Element A at (%)	Element B at (%)	Element C at (%)	Element D at (%)	Melting point (°C)
Ga	100	0	0	0	29.8
Ga/In (EGaIn)	85.8	14.2	0	0	15.4
Ga/Sn	91.7	8.3	0	0	21.0
Ga/Al	97.6	2.4	0	0	25.9
Ga/Zn	96.1	3.9	0	0	24.7
Ga/Hg	98.0	2.0	0	0	27.0
Ga/In/Sn (galinstan)	78.3	14.9	6.8	0	13.2
Ga/In/Zn	67.0	29.0	4.0	0	13.0
Ga/In/Sn/Zn	51.0	25.0	13.0	1.0	3.0

SiO_2/Si wafers or polyimide films.[37] The non-polar and mobile nature of the parent metal also make the oxide skin on the surface less attractive, allowing for easy transfer of the oxide layer to desired substrates or its layering into a colloidal suspension (Fig. 3c). Moreover, this facile method to acquire 2D metal oxides is not limited to single-phase metal surfaces. Integrating desired metal elements into LMs can create alloys, and on the surface of LM alloys, metal elements compete for presence in the 2D oxide layer. The oxide that leads to the largest reduction in Gibbs free energy (ΔG_f) will dominate the surface, allowing controllable modification of the oxide layer by the addition of different selected metals (Fig. 3d).[35]

2.4 Ultra-smooth and "layer" surface

Interestingly, upon the removal of oxide skin (*i.e.*, with acid), LMs feature an atomically smooth and highly reactive surface, characterized by abundance of many quasi-free electrons and positive ions.[2] The ultra-smooth surface template characteristic of LMs makes them exceptionally suitable for the deposition of 2D layered materials. Such a surface offers significant advantages, including prevention of inhomogeneous nucleation, minimization of defects and reduction of grain boundary occurrence (Fig. 3e).[52,53] Moreover, near the surface of LMs, there is a relaxation in interatomic interactions, differing from those in the metal core. The variation leads to a change in density from the body of the metal to the liquid–gas interface, resulting in the liquid core of the metal exhibiting a state of almost free electrons, while the surface becomes layered and ordered (Fig. 3f).[2,40] This surface "layering", typically only two to three atomic diameters thick, is observed in many oxide-free LMs and their alloy droplets.[39] This surface structure plays a crucial role in the distinctive properties and applications of LMs, particularly in the field of low-dimensional materials synthesis.

3 Liquid metal reactors for nanomaterials synthesis

3.1 Metallic nanomaterials

3.1.1 Solid metallic nanomaterials. Ga-based LMs possess an extraordinary ability to dissolve a diverse range of elements, making them ideal liquid media for reactions that lead to the creation of innovative products.[40,41] The variety of solute

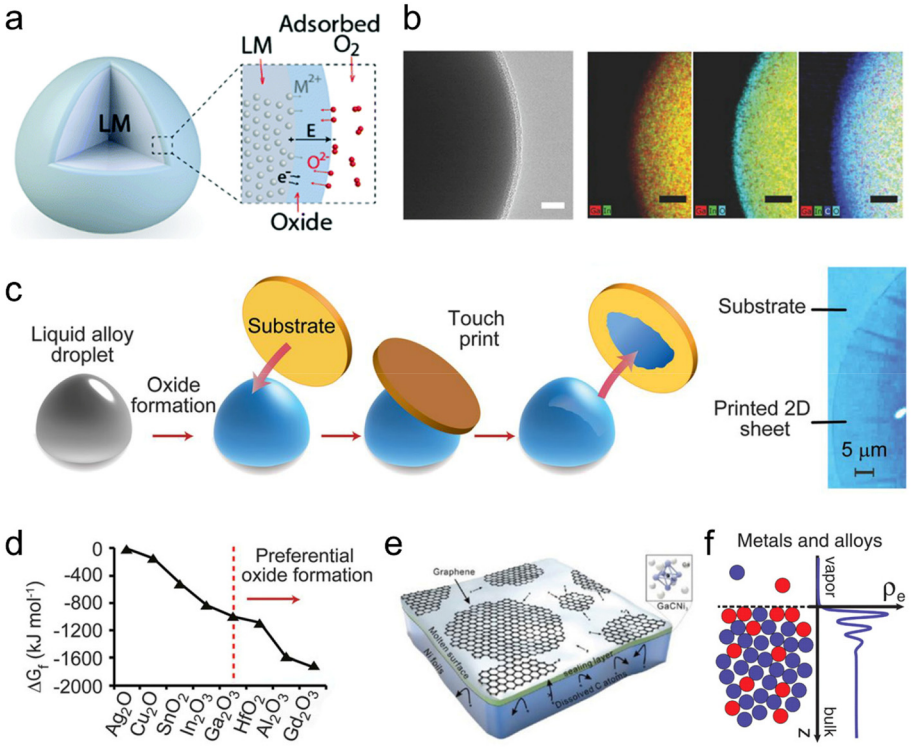

Fig. 3 Unique surface properties of Ga-based LMs. (a) Schematic diagram of the Cabrera–Mott metal oxidation model. Reprinted with permission.[16] Copyright (2021), Royal Society of Chemistry. (b) TEM image and elemental mapping of the EGaIn nanoparticles with an oxide skin. Scale bars are 5 nm for the TEM image and 10 nm for the elemental mapping. Reprinted with permission.[33] Copyright (2015), Wiley-VCH. (c) Schematic of oxide layer exfoliation and translocation on LMs. (d) ΔG_f of formation for different metal oxides. The oxides leading to the maximum reduction in ΔG_f (to the right of the red dashed line) are predicted to dominate the interface. Reprinted with permission.[35] Copyright (2017), American Association for the Advancement of Science. (e) Chemical vapor deposition (CVD) growth of 2D $GaCNi_3$ on the liquid Ga ultra-smooth surface. Reprinted with permission.[38] Copyright (2015), American Chemical Society. (f) Schematics of the atomic surface structure and electron density profile $\rho_e(z)$ of LMs. Surface layered structures are observed for both metals and alloys. Reprinted with permission.[39] Copyright (2006), American Association for the Advancement of Science.

elements that can be dissolved in LMs includes post-transition metals,[42] transition metals,[43] lanthanides,[44] elements from the zinc group,[45] alkali metals,[46] rare earth elements[47] and some semi-metals (Fig. 4a).[20] Ga-based LMs can react with other metals to form alloys or composites through thermal[48] and mechanical forces,[49] electric fields[50] and micromachining (Fig. 4b).[51] Furthermore, the composition of binary, ternary, or more complex metallic element LM alloys or composites can be predicted through an integration of phase diagram calculations, theoretical analyses, experimental justifications and computational simulations (Fig. 4c).[52]

Additionally, Ga possesses a low standard reduction potential, allowing it to undergo galvanic replacement with a wide range of metals. This unique attribute makes Ga-based LMs a versatile template for GRR. Leveraging this, bimetallic nanoparticles (NPs), metallic crystals or metal shells in their reduced state can be synthesized through the GRR. The reaction is controlled by the disparity in the standard reduction potentials between the two metal/metal ion couples involved,[55] such as Ga with Cu^{2+}, Ag^{+}, Co^{3+}, Ni^{2+}, Cd^{2+}, Sn^{2+}, Pt^{2+}, Au^{3+} and others (Fig. 5a).[27,55–57] Notably, recent studies highlight the efficiency and versatility of sonochemical synthesis in producing Ga-based nano-alloys.[49] Sonochemical-assisted synthesis, when applied in metal-ionic solutions, facilitates the growth of crystalline nanostructures on the surface of LM NPs,[13] such as 1D Ag–Ga nano-alloys (Fig. 4b and 5b),[6] binary and ternary alloy nanoparticles (Fig. 5c),[56] and core–shell nanoparticles (LM core and WO_x, MoO_x, VO_x, MnO_2 shell) (Fig. 5d).[58] These nanostructures or nanoparticles can be optimized by fine-tuning the chemical concentration, the sequence of addition and introducing oxidizing skin inhibitors. When modulating the sonochemical-assisted GRR process of a Ga–chloroauric acid ($HAuCl_4$) system and adding NaH_2PO_4 inhibitors, unprecedented Au@Ga oxide and hollow Ga oxide nanostructures were obtained.[59] Bimetallic NPs, synthesized through the GRR strategy with Ga, such as Ga–Pd, Ga–Pt and Ga–Ni, find diverse applications in catalysis and photocatalysis.[56,60,61] Furthermore, this approach can further create metal-shelled or hollow-shelled nanoparticles, which hold promise for various applications, including nanoreactors,[62] catalysis,[63] drug delivery[64] and diagnostic imaging.[65]

Intriguingly, when a solute metal is fully dissolved in a Ga solvent at high temperatures and subsequently becomes supersaturated upon cooling, intermetallic crystals composed of Ga

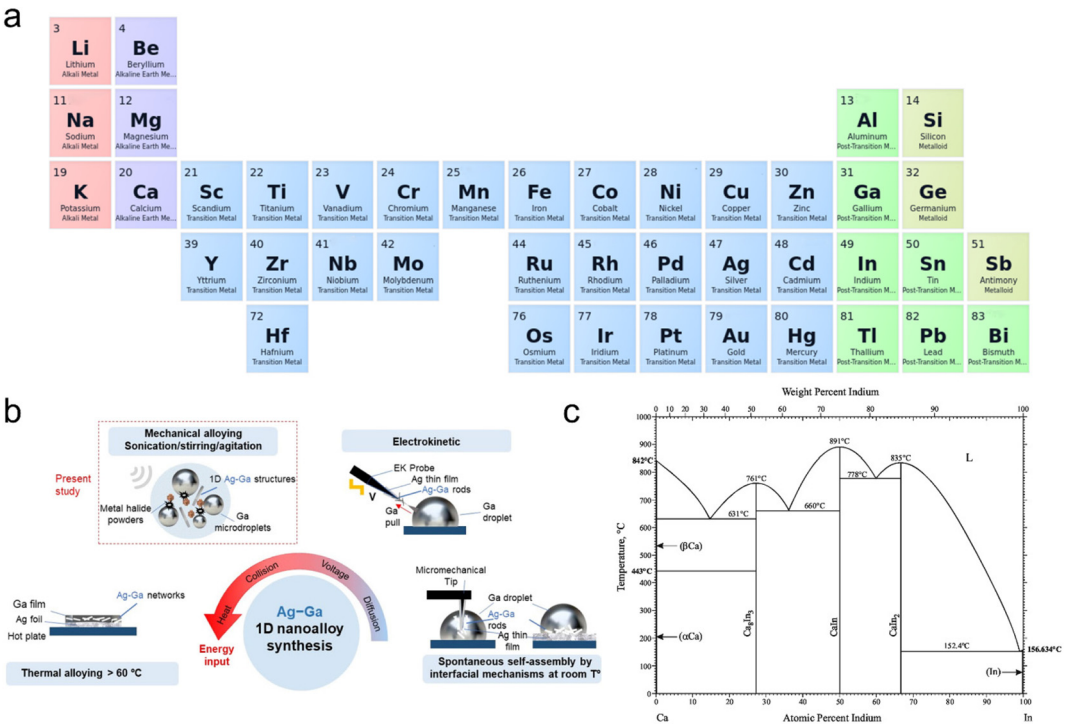

Fig. 4 Liquid Ga can serve as a reaction medium. (a) Elements that may get dissolved in Ga.[4,53] (b) Schematic representation of the synthesis methods of the LM alloy, taking Ag–Ga alloys as an example. Reprinted with permission.[6] Copyright (2022), American Chemical Society. (c) Analyzed Ca–In phase diagram alongside the corresponding experimental data. Reprinted with permission.[54] Copyright (2016), ASM International.

and the solute metal can crystallize within the LMs.[9] Physical perturbations at the interfaces of LMs, such as applying electric potential or controlling the melting temperature, can induce phase separation of solute metals into their zero-valent form, a phenomenon known as 'metal expulsion'. This results in the complete separation of metal entities from the LMs. For example, alloys, such as Ga–In–Sn and In–bismuth (Bi)–Sn, can be utilized as electrochemical cathodes to initiate the separation of the metal phases at the LM–electrolyte interface by applying a cathodic potential, with the type of metal emission depending on the electrolyte (Fig. 5e–g).[8] Moreover, the interfacial crystal formation within metallic liquid–solid coexisting systems leads to unique growth dynamics, crystal structures and arrangements that are distinct from traditional solvent precipitation (Fig. 5h). This LM-based intermetallic crystal growth approach holds promise for designing bimetallic or multi-metal structures useful for catalysis,[66] sensing[67] and energy storage.[11,68]

3.1.2 Nanoporous metals. An alternative application of the excellent alloying properties of Ga-based LMs is in the production of nanoporous metals. In this process, a single component of a binary alloy within the Ga-based LM can be selectively dissolved to produce nano-porous materials, known as a dealloying process. This involves liquid Ga reacting with a solid metal to form crystals, followed by selective removal of the less inert and relatively soft Ga from the intermetallic crystals, thereby creating a nanoporous metal (Fig. 6a).[11,69] For instance, liquid Ga is used as a metal solvent to grow intermetallic crystals by integrating solid transition metal copper (Cu), silver (Ag), gold (Au), palladium (Pd) and platinum (Pt) substrates.[11] Subsequently, Ga is selectively removed to design transition metal-based nanoporous metals *via* chemical and electrochemical dealloying methods, due to its low standard reduction potential compared to many transition metals (Fig. 6c). Pore size analysis reveals the uniform formation of nanoligaments and pores in single- or double-digit nanometer sizes (Fig. 6b and d).[11] When the inert metal substrate is a thin film, the liquid Ga-assisted alloying–dealloying strategy is also employed to design porous metal films with tunable porosity and thickness.[70] This low-temperature method allows accessibility to well-controlled nanoporous metals, offering scalability and low energy costs.[71] The resulting nanoporous metals are crucial in diverse applications, including catalysts,[72] actuators,[73] sensing/biosensing[74,75] and energy systems,[76] owing to their bicontinuous channel-ligament structure and high surface area.

3.1.3 High-entropy nanoalloys. High entropy alloys (HEAs) are a unique category of alloys notable for their high configurational entropy of mixing, often surpassing the enthalpy of formation of the compound, which leads to be the formation of single-phase disordered solid solutions. These alloys are known for their excellent chemical and mechanical properties, including robust mechanical strength, high thermal stability, superior oxidation and corrosion resistance, as well as exceptional biocompatibility.[77–79]

The easy alloying properties of Ga-based LMs, coupled with the negative mixing enthalpy with other metal elements, make

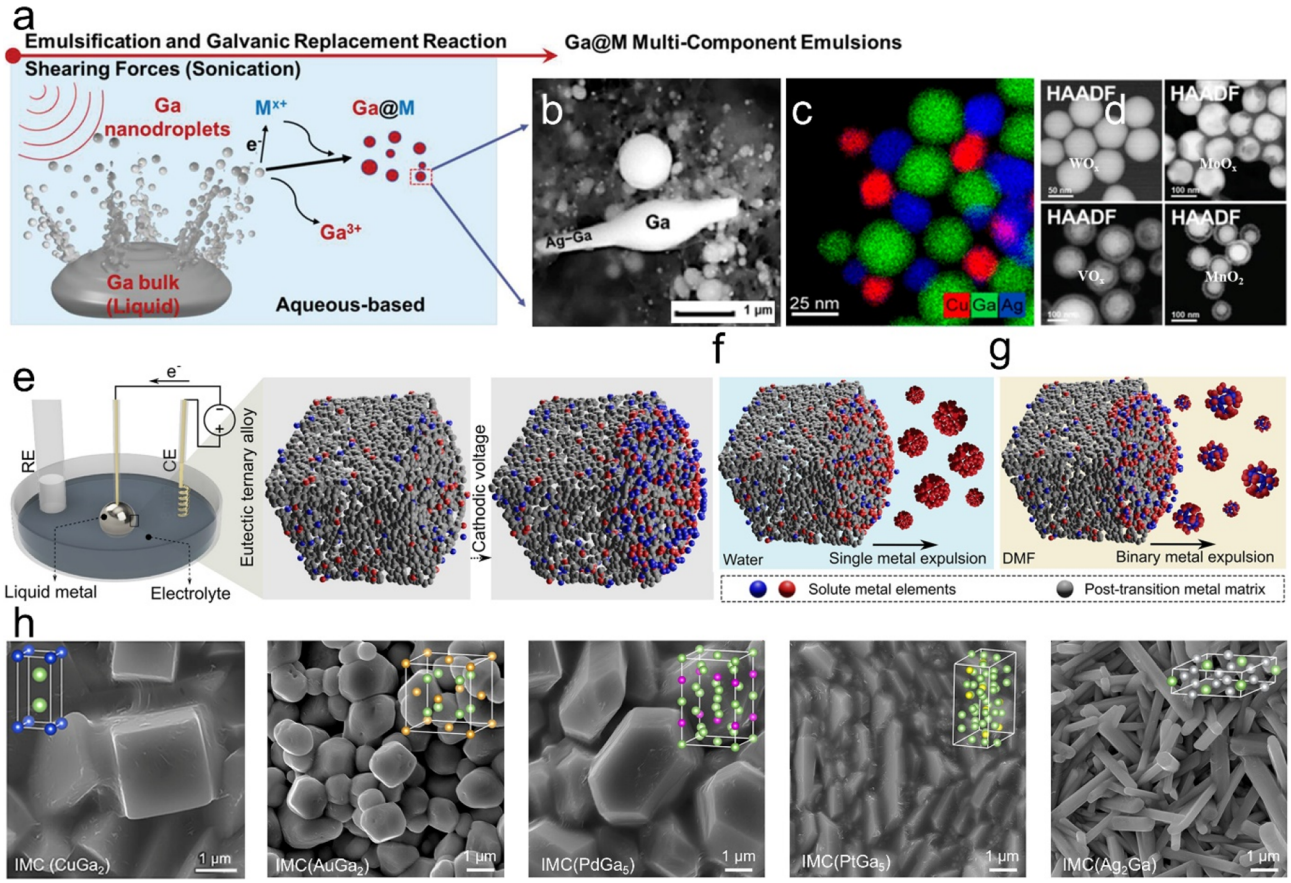

Fig. 5 Galvanic replacement reaction (GRR) and metal expulsion based on the liquid Ga system. (a) Schematic of the ultrasound induced GRR between metal ions and Ga. Metal salt ions (M^{x+}) are reduced by Ga to form Ga@M bimetallic composites. Reprinted with permission.[58] Copyright (2021), Wiley-VCH. (b) High-magnification SEM (HM-SEM) images of typical 1D Ag nanoneedles with Ga nanoparticles. Reprinted with permission.[6] Copyright (2022), American Chemical Society. (c) Energy dispersive X-ray spectroscopy (EDXS) elemental maps of Ag–Cu–Ga ternary alloy nanoparticles. Reprinted with permission.[56] Copyright (2020), American Chemical Society. (d) High-angle annular dark-field (HAADF) image of the Ga core and WO_x, MoO_x, VO_x and MnO_2 shells. Reprinted with permission.[58] Copyright (2021), Wiley-VCH. (e) Schematic diagram of an electrochemical device for applying an electrical potential to the Ga alloy surface. Expulsion of the (f) monophasic metals in aqueous electrolytes and (g) binary metals in non-aqueous electrolytes. Reprinted with permission.[8] Copyright (2022), American Chemical Society. (h) SEM images of $CuGa_2$, $AuGa_2$, $PdGa_5$, $PtGa_5$ and Ag_2Ga intermetallic crystals. Reprinted with permission.[11] Copyright (2023), American Chemical Society.

them an ideal matrix for preparing complex multicomponent HEAs.[80] Specifically, the negative mixing enthalpy can reduce the ΔG_f, enabling effective creation of homogeneous alloys through liquid Ga-assisted synthesis methods, overcoming the challenges of elemental segregation and immiscibility in alloy systems. For instance, it is feasible to create an equiatomic HEA of gallium, indium, tin and zinc (GaInSnZn) by employing a technique that involves induction-melting high-purity elements of In, Sn and Zn in equal ratios (1 : 1 : 1) within a Ga solvent (Fig. 7a). The resulting HEA is a highly conductive fluid, promising for flexible electronic applications (Fig. 7b).[81] Additionally, a novel and versatile strategy has recently been developed for synthesizing HEA NPs from various metal elements (Cu, Pd, Ni, Mn, Al, In, Rh, Pt, Co and Mg) with Ga-based LMs as reaction media and reservoirs under mild conditions (923 K) (Fig. 7c and d).[82] Ga's relatively negative mixing enthalpy with other solute elements results in HEAs with a highest percentage of solid solution for compositions with the same mixing enthalpy (Fig. 7e).[82] This method represents a significant advancement in the field of materials science, particularly in the synthesis of HEAs, enabling the creation of customizable metal nanoparticles under mild conditions. The nanostructures of HEAs, with their high specific surface area, strong synergistic effects, customizable compositional variations and significant lattice distortions, expand their potential applications.[82,83] This facile strategy makes them an ideal platform for a variety of surface reactions,[84,85] making them applicable in fields such as multiphase catalysis,[83] energy storage[86] and bio/plasma imaging.[86,87]

3.1.4 Metallic single atoms. Single atoms (SAs) exhibit exceptional performance in numerous catalytic reactions owing to maximized atom utilization, high catalytic selectivity and distinct coordination environments.[88,89] However, developing a universal, efficient, and controllable synthesis method for single atoms is challenging due to the high surface energy of individual atoms.[90] Traditional synthesis methods often

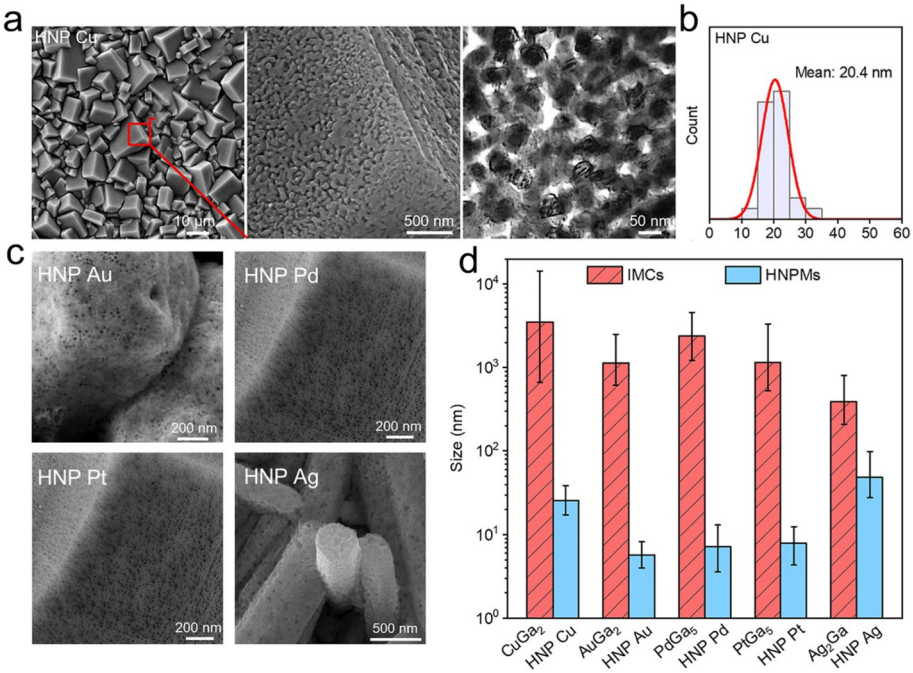

Fig. 6 Porous characterization of hierarchical nanoporous metals. (a) SEM and TEM images of hierarchical nanoporous (HNP) Cu show the micro/submicro cuboids decorated with nanoscale ligaments and pores. (b) Pore size distribution of the Cu indicates nanoscale ligaments and pores of about 20.4 nm. (c) SEM images of the nanoporous Au, Pd, Pt and Ag reveal the versatility of this strategy. (d) Characteristic sizes of the hierarchical porosities of intermetallic crystals and HNP metals. Reprinted with permission.[11] Copyright (2023), American Chemical Society.

require harsh conditions or lengthy processes.[60] Notably, the potent reducibility and fusible properties of Ga-based LMs offer a promising solution for effectively dispersing individual atoms.[91]

Ga single atoms, with their inherent catalytic properties, can be prepared through impregnation and reduction under a high temperature atmosphere.[91–93] For instance, Ga SAs were successfully synthesized by reducing Ga metal salt precursors under a high temperature atmosphere. The confinement effect of oxygen vacancies (V_O) plays a crucial role in this process, favoring the synthesis of well-isolated Ga SAs. This results in maximizing the availability of Ga–V_O reaction sites, thereby significantly enhancing catalytic activity and selectivity.[92] Another example is the creation of Ga single atom-coordinated hollow ZSM-5 catalysts *via* wet chemistry combined with high-temperature treatment. These encapsulated Ga SA catalysts exhibit high catalytic conversion efficiency, excellent reusability, and resistance to sintering, attributed to the presence of Ga single atoms.[93] Besides the high-temperature and wet-chemical synthesis strategies, laser irradiation is a more facile and effective method to synthesize Ga SAs at room temperature.[91] Additionally, the fluid nature of the LMs enables the mobility of Ga single atoms, and a series of Ga single atoms with different coordination environments (P, S and N atom doping) have been synthesized (Fig. 8a and b). The fluxional feature of Ga single atoms enhances the active sites, improving catalytic stability and boosting activity in CO_2 reduction for CO formation.[94]

Besides Ga SAs, the metal-fluid nature of Ga-based metal alloys results in solute elements to be atomically isolated, resembling solute single atoms of other metallic elements (Fig. 8c). For instance, in a Ga–platinum (Pt) catalyst, liquid Ga serves as a support matrix for Pt, and these Pt atoms are uniformly dispersed within the liquid Ga matrix, effectively preventing atomic aggregation and resulting in the formation of "liquid" Pt single atoms (Fig. 8d). This unique catalytic system accelerates various catalytic reactions and significantly improves kinetics at low temperatures.[95] Similarly, in the $GaSn_{0.029}Ni_{0.023}$ liquid alloy catalyst, the Ga solvent plays a crucial role in achieving well-dispersed tin (Sn) and nickel (Ni) atomic configurations, resulting in a highly selective catalytic synthesis of propylene (Fig. 8e).[96] In addition, liquid Ga also assists in generating Pd single atoms through physical vapor deposition of Pd–Ga alloys in an ultrahigh vacuum environment.[97] An another notable aspect of liquid Ga is its abundant vacancies, which allow it to incorporate various metallic elements as a second phase. Within this system, the active second-phase element is dynamically and atomically isolated within the liquid Ga-rich phase of these binary eutectic alloys, contrasting with solid metals. Such alteration in their electronic structure leads to significantly enhanced catalytic properties, offering possibility in future studies to use lower energies (under mild conditions) for breaking metal bonds to obtain various SAs. Furthermore, the liquid matrix provides exceptional fluidity, deformability and self-healing capabilities, beneficial for product separation, maintaining catalytic

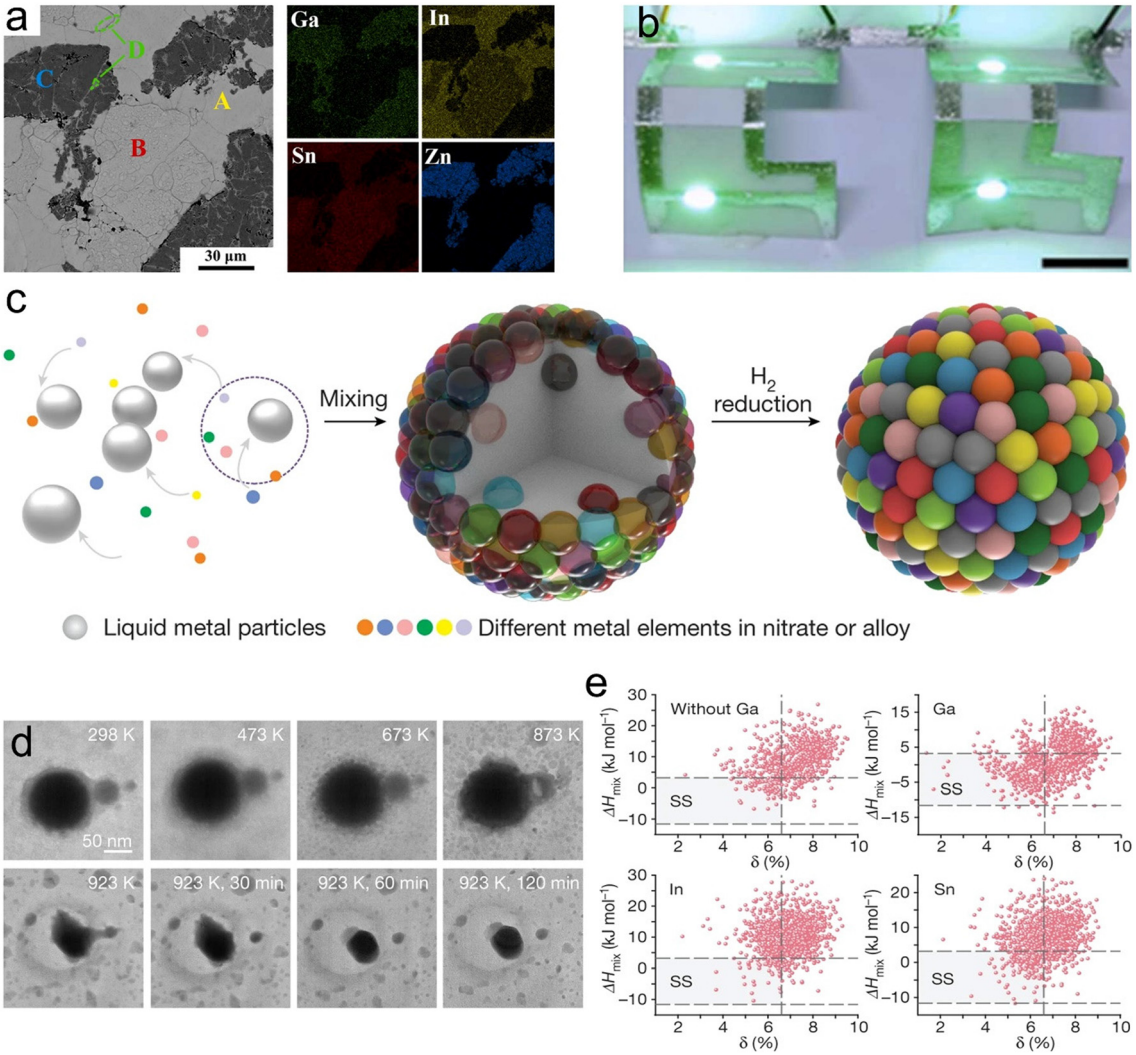

Fig. 7 Ga-based high entropy alloys (HEAs). (a) Back scattering electron (BSE) image of GaInSnZn HEAs; elemental mapping shows that the components in the alloy are phase separated. (b) GaInSnZn-based direct-writing 3D electronic circuits; scale bar is 2 cm. Reprinted with permission.[81] Copyright (2022), Elsevier B.V. (c) Schematic diagram of the LM reservoir-assisted synthesis process for HEA NPs. Various metal salt precursors are mixed, thermally decomposed, hydrogen reduced and alloyed in liquid metal reservoirs. (d) The TEM image of the process of conversion from precursors into HEA NPs shows that the HEANPs were formed on a large scale after 30 min at 923 K. (e) The distribution of the mixing enthalpy (ΔH_{mix}) and the atom radii difference factor (δ) of the HEAs without Ga and containing Ga, In and Sn. With the introduction of Ga, more data points were available to satisfy the ΔH_{mix} and δ in the solid solution phase region. Reprinted with permission.[82] Copyright (2023), Springer Nature.

system integrity even in the face of external damage and reducing interface polar impedance. For example, dynamic dispersion of Sn atoms in the liquid Ga matrix can maintain long-term integrity of the catalytic conversion of lithium polysulfides (LiPSs), thereby improving their overall catalytic performance.[98]

3.2 Metal compound nanomaterials (inorganics)

3.2.1 Metal oxide nanomaterials (2D materials). Ga-based LMs feature a self-limiting thin oxide layer under ambient conditions at the metal–air interface, which is considered to be one of the most perfect 2D planar materials.[31] Ga spontaneously forms oxides in ambient air and the oxidation process follows the Cabrera–Mott oxidation model.[35,99,100] Factors such as the metal's work function, the process temperature and the oxide properties influence the oxide layer's morphologies and thickness.[16,31] For instance, Ga_2O_3 forms a layer of about 0.5 nm on Ga when exposed to an oxygen dose of more than 8×10^{-6} Torr.[30] Ga_2O_3 printed from Galinstan surfaces is amorphous and 2.78 nm thick, while it is ~3 nm on amorphous EGaIn and Galinstan nanoparticles with a self-assembled organic thiol layer.[16,35] The thiolate modification effectively mitigates the growth of the oxide layer on the surface of EGaIn particles, and the thickness of the oxide layer can be controlled between 1.23 and 2.12 nm (Fig. 9a–c).[101] In addition to the spontaneous oxide formation, 2D hexagonal ribbons of Ga_2O_3 single crystals (tens of nanometers thickness) can be grown on liquid Ga in a controlled manner by sublima-

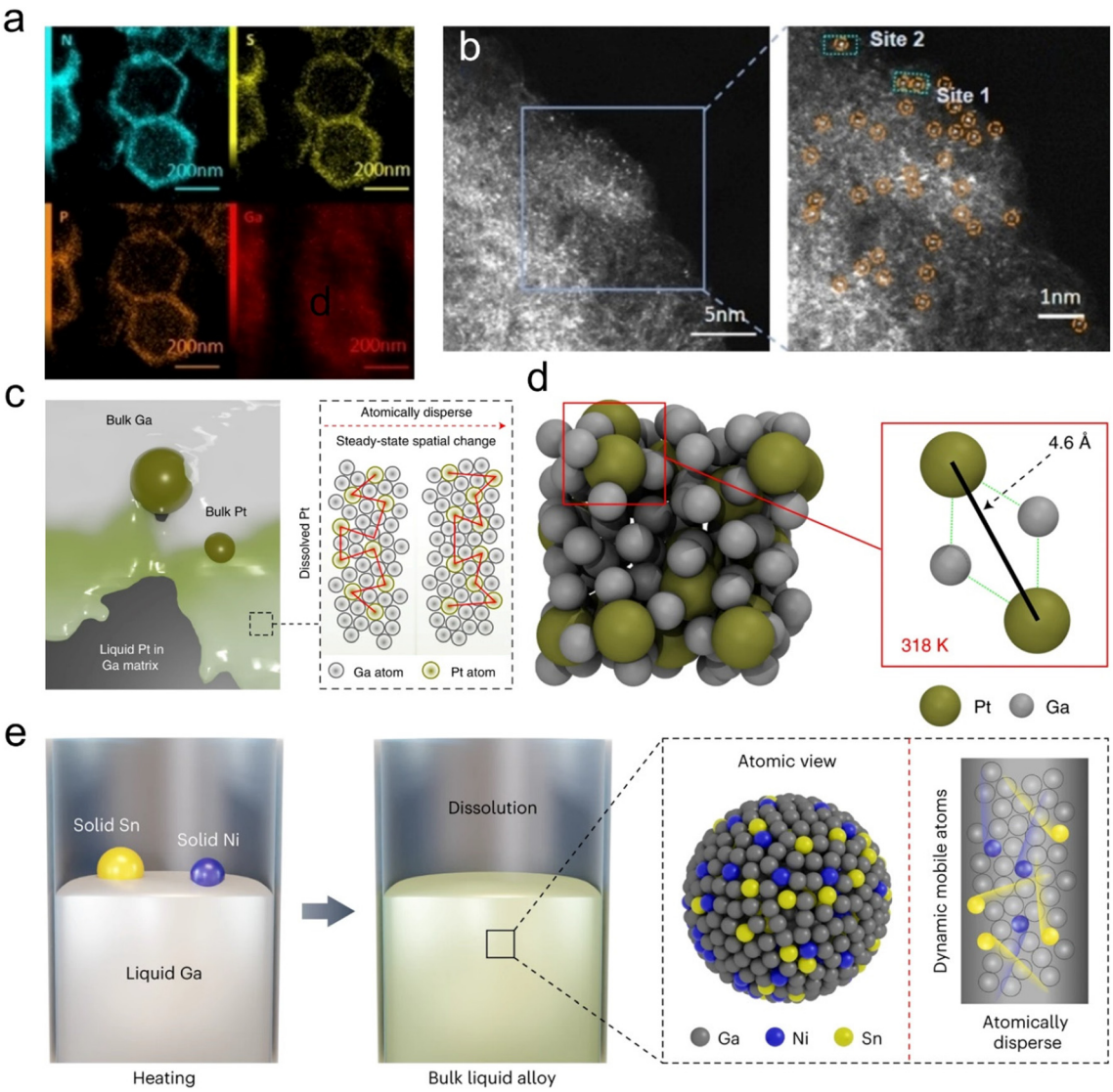

Fig. 8 Ga single atoms (SAs) or metal SAs produced with Ga assistance. (a) EDS elemental mapping of the Ga-N_3S-PC catalyst confirms the distribution of P, S, N, and Ga elements. (b) The atomic phase image of the Ga-N_3S-PC catalyst shows the dispersed Ga single atoms. Reprinted with permission.[94] Copyright (2022), Wiley-VCH. (c) Schematic representation of the Ga–Pt system and its atomic distribution. Pt is atomically dispersed and maintains dynamics in Ga solvents. (d) Representative snapshots of the atomic configurations of Pt in Ga in the bulk. Two Pt atoms dispersed in Ga are 4.6 Å apart, indicating that Pt remains in the liquid state. Reprinted with permission.[95] Copyright (2022), Springer Nature. (e) Schematic representation of the preparation and atomic mobility of the liquid $GaSn_{0.029}Ni_{0.023}$ catalyst. Sn and Ni remain atomically dispersed and active in the Ga matrix. Reprinted with permission.[96] Copyright (2023), Springer Nature.

tion of O atoms at 1020 °C using chemical vapor deposition (CVD) (Fig. 9d–f).[102] More importantly, the surface oxide of Ga-based LMs exhibits minimal adhesion to the parent metal in a liquid state, allowing easy transfer to other substrates *via* van der Waals (vdW) transfer techniques.[35,37,103]

Furthermore, the alloying of Ga-based LMs allows the formation of co-alloyed 2D metal oxides at the LM–air interface.[35] In these LM alloys, the surface oxides are determined by the oxide with the lower Gibbs free energy, typically leading to a binary oxide on the surface.[104] Moreover, the oxides that lead to the largest reduction in ΔG_f are the main products, and LM eutectic alloys, such as EGaIn, mainly consist of Ga oxides in their surface oxide composition (Fig. 10a).[105] However, selecting specific alloying elements can control the oxide layers, allowing the spontaneous formation of high-melting-point oxides like HfO_2, Gd_2O_3 and Al_2O_3, instead of Ga_2O_3 (Fig. 10b), and XPS shows exfoliated 2D materials consisting entirely of oxides of solute elements (Fig. 10c). This method offers a controllable method to synthesize high-quality 2D metallic oxides at or near room temperature.[35] Notably, this principle could be extended to other LMs (*i.e.*, Sn–Bi alloys and Bi–Sb alloys) to obtain Bi_2O_3-doped SnO nanosheets and ultra-thin α-Sb_2O_3 layers, respectively.[106,107] For further examples and detailed insights into metal oxide synthesis using non-Ga-based LMs,

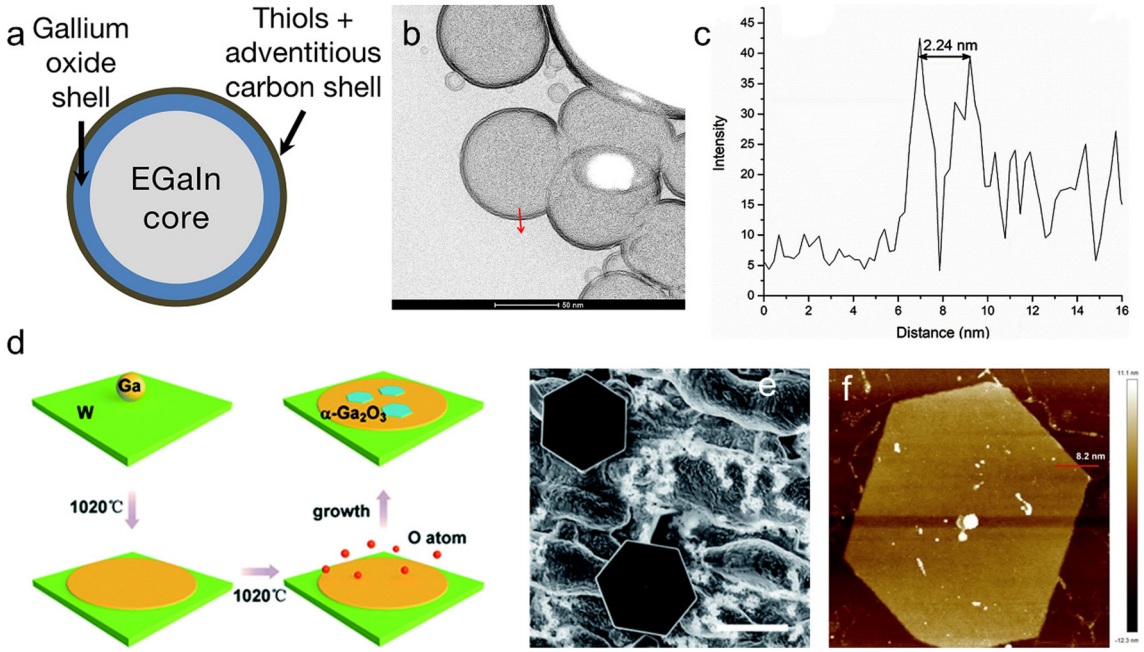

Fig. 9 Ga oxide layer, 2D Ga_2O_3. (a) Schematic showing thiolated molecule functionalized EGaIn nanoparticles. (b) Representative HAADF image of 1-day old thiophenol-functionalized EGaIn nanoparticles after processing with a sobel filter to reveal Ga oxide shell thickness. (c) Intensity peaks extracted from scanning transmission electron microscopy (STEM) images of the nanoparticles. The average Ga oxide shell thickness values were $h_{TP,1day}$ = 1.23 ± 0.20 nm and $h_{TP,28days}$ = 2.12 ± 0.26 nm. Reprinted with permission.[101] Copyright (2018), American Chemical Society. (d) Schematic diagram of the growth process of hexagonal α-Ga_2O_3 crystals. As the temperature increases, Ga spreads out on the substrate to form a flat surface, and O atoms diffuse into the surface of liquid Ga to form hexagonal α-Ga_2O_3. (e) The SEM image shows that the Ga_2O_3 crystals are regular hexagonal in shape and extremely homogeneous. (f) Atomic force microscope (AFM) image of the hexagonal Ga_2O_3 crystals. Reprinted with permission.[102] Copyright (2021), Royal Society of Chemistry.

readers are encouraged to consult recent reviews on this topic.[17,21]

Interestingly, in the presence of different temperatures, Galinstan undergoes a transition from self-limiting Cabrera–Mott oxidation to a more complex, non-self-limiting reaction, forming heterogeneous oxide regions or shells containing Ga, In and Sn.[16,108,109] The formation of LM oxides is influenced by several factors: (1) Temperature. Temperature plays a crucial role, as higher temperatures boost oxidation through increased thermal energy and favorable thermodynamics. (2) Environment. The environmental conditions, particularly the presence and pressure of oxygen, significantly impact the rate of oxidation. (3) Interfacial properties. Interfacial properties including surface contaminants, tension, and wetting determine oxide layer morphology and thickness. (4) LM composition. The composition of the LM, along with dissolution kinetics, and mechanical aspects influence oxide skin formation. By controlling these factors, it is possible to tailor LM oxides for specific applications and uses.[109] Furthermore, oxide layers can be acquired by introducing gases into LM melts in various environments (such as aqueous, organic, or inorganic electrolyte solutions) to go beyond self-limiting oxidation. For instance, GaOOH microcrystals form when liquid Ga is sonicated in the presence of water,[110] while γ-AlOOH is synthesized through the interaction of the Galinstan–Al alloy surface with water.[111]

Liquid Ga serves as an excellent template for 2D material growth due to its atomic-level ultra-smooth surface and strong reducibility.[2] In acidic solutions, the Ga surface readily attracts H^+ to exhibit a dynamic electric double layer (EDL) (Fig. 10d).[18,112] The self-generated potential, along with excess electrons on the Ga surface, provides an ideal environment for reducing metal anions at the interface.[112] One notable example is the reduction of the molybdate precursors (MoO_4^{2-}) templated onto the liquid–liquid interface, leading to the formation of hydrated molybdenum oxide (H_2MoO_3) (Fig. 10e). These are subsequently transformed into 2D MoO_2 *via* laser writing techniques (Fig. 10f).[112] Similarly, atomic-thickness hydrated MnO_2 sheets and the inorganic network of nano-MnO_2 are synthesized by an electric coupling substitution reaction between permanganate ions and EGaIn.[12,113] Additionally, 2D CuO_x nanomaterials are produced by galvanic replacement between $Cu(OH)_3^-$ and liquid Ga.[14] The electron accumulation on the Ga surface creates a reactive surface potential, driving the reduction and self-deposition of precursor metal cations. For example, significantly crystallized rhombohedral layered Bi_2Te_3 platelets were formed when metal-based cations (specifically Bi^{3+}–$HTeO_2^+$ in acidic environments) are introduced to the smooth and oxide-free EGaIn surfaces.[114] These 2D metal oxides derived from Ga-based LMs have been explored for a variety of potential applications, including electronic devices,[115] spintronics,[116] photocatalysts,[117] energy storage

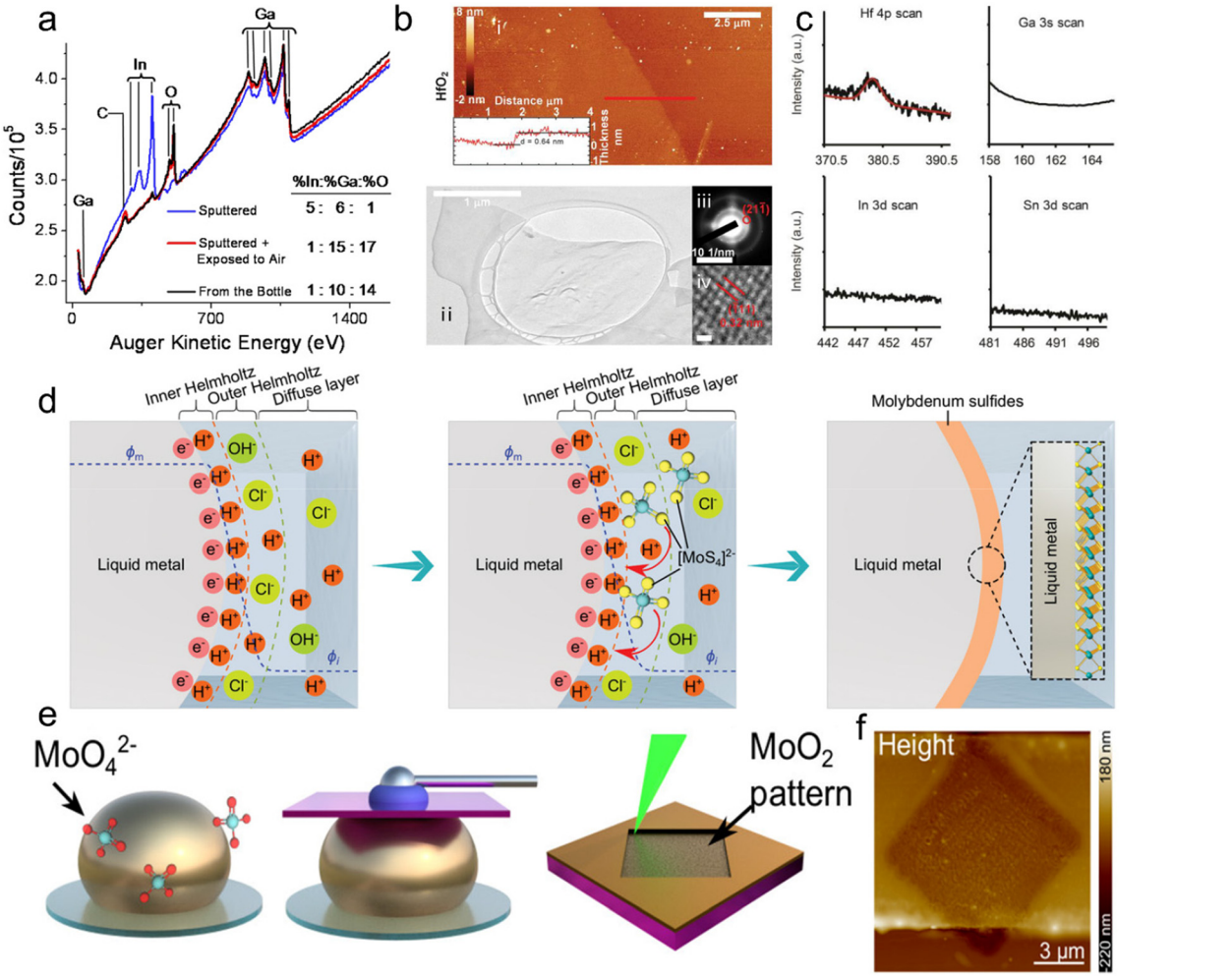

Fig. 10 2D metal oxides formed on the LM alloy surface and metal oxides produced by the reaction of electrolyte solutions with LM surfaces. (a) Auger spectra of EGaIn samples from the bottle (black), removed from the outer skin (blue) and exposed to air after removing outer layer. It shows that the oxide layer of EGaIn is mainly composed of Ga_2O_3. Reprinted with permission.[105] Copyright (2008), Wiley-VCH. (b) Characterization of metal oxides from the GaInSn alloy containing 1% Hf. i, AFM images, with thickness profile (inset) determined at the red line as indicated. ii, TEM image. iii, selected-area electron diffraction (SAED). iv, high-resolution TEM images (scale bar, 0.5 nm). The as-grown HfO_2 sheets are ultrathin and polycrystalline. (c) XPS spectra of the exfoliated metal oxides from the GaInSn alloy containing 1% Hf shows that the oxides are composed exclusively of HfO_2. Reprinted with permission.[35] Copyright (2017), American Association for the Advancement of Science. (d) Schematic diagram showing dynamic electric double layer (EDL) formation on LM surfaces, where $[MoS_4]^{2-}$ reacts with H^+ in the Helmholtz layer to form 2D MoS_2. Reprinted with permission.[35] Copyright (2020), Wiley-VCH. (e) Schematic diagram of the preparation and patterning process of the 2D MnO_2 material. MnO_2 was prepared by introducing molybdate precursors around EGaIn droplets. A laser writing technique was used to prepare patterned MnO_2. (f) AFM image of the laser-annealed pattern shows 45 nm reduction in thickness. Reprinted with permission.[112] Copyright (2021), American Chemical Society.

systems,[118] sensors[119] and more,[120,121] highlighting their versatility and potential in various technological fields.

3.2.2 Other 2D materials (metal sulfides, phosphates, nitrides, selenium, *etc.*). The unique reaction conditions at the interface of liquid metals (LMs) not only facilitate the 2D growth of both layered and non-layered metal oxides, but also extend to the synthesis of other 2D compounds like sulfides,[122] phosphates[123] and nitrides[124] directly on the LM surface under anoxic conditions (Fig. 11a).[16] This LM-based method offers significant advantages over traditional exfoliation and 'bottom-up' techniques, including faster processes and eliminating the need for meticulous control of epitaxy conditions and surfactant-mediated growth.[35] For instance, tin sulfide (SnS) forms spontaneously *via* the Cabrera–Mott sulfurization, using a custom-built device exposing liquid Sn droplets to an anoxic environment of H_2S gas at 350 °C. The resulting SnS lamellae can be stripped off from the LM surface and transferred to another substrate by vdW adhesion.[125,126] Similarly, homogeneous tetragonal In_2S_3 with a single unit cell thickness is synthesized by exposing it to sulfur vapor under nitrogen flow.[28] Additionally, high-quality and nanoscale-thick 2D GaN films are created by direct nitridation of Ga droplets through exposing to N_2 plasma at room temperature (Fig. 11a–c).[127]

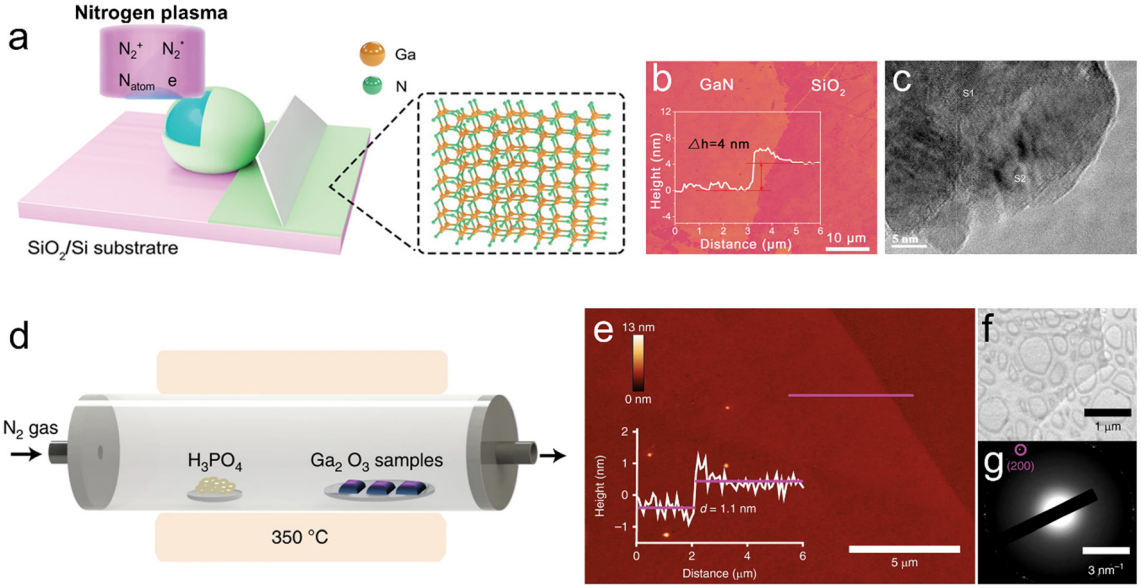

Fig. 11 2D GaN semiconductors were directly derived from LM Ga and $GaPO_4$ nanosheets were transformed from Ga_2O_3. (a) Schematic illustration of the formation of a GaN layer on Ga *via* a nitrogen-plasma reaction mechanism. The GaN layer adheres to the substrate by vdW forces. (b) AFM image shows the exfoliated GaN layer at 4 nm height. The inset shows the step height profile of the GaN layer. (c) High-resolution TEM images confirm the crystallization of the GaN nanosheets. Reprinted with permission.[127] Copyright (2022), Wiley-VCH. (d) Schematic diagram of the vapor phase reaction system for the synthesis of $GaPO_4$ nanosheets. (e) AFM topography of a $GaPO_4$ nanosheet and the height profile along the magenta line. (f) TEM micrograph of the $GaPO_4$ film shows a translucent sheet-like morphology. (g) The SAED pattern of the TEM micrograph of the $GaPO_4$ nanosheet confirms its crystalline structure. Reprinted with permission.[103] Copyright (2018), Springer Nature.

Additionally, other chemical modifications or CVD vapor conversion of Ga_2O_3 can produce other 2D materials. For instance, centimeter-scale Ga_2O_3 is produced through substrate printing methods, followed by a chemical vapor-phase reaction with phosphoric acid to form 2D $GaPO_4$ nanosheets (Fig. 11d–g).[103] Similarly, chlorination and low-temperature sulfurization steps can transform Ga_2O_3 and In_2O_3 into 2D GaS and In_2S_3, respectively.[115] Extrusion printing and ammo-

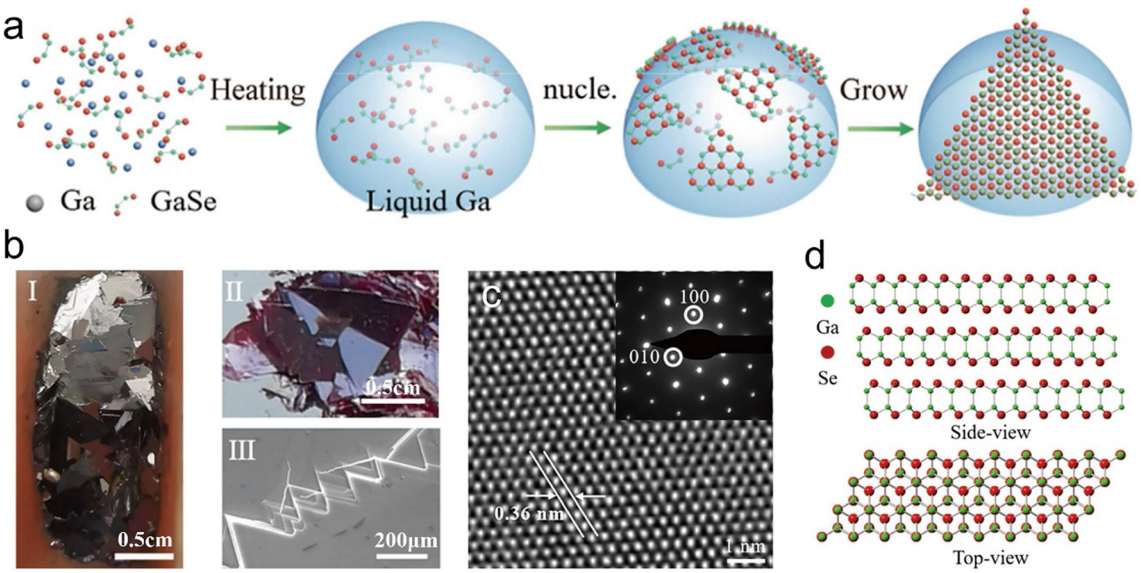

Fig. 12 The growth of GaSe crystals on the liquid Ga surface. (a) Schematic representation of the GaSe 2D crystal formation process. GaSe powder melts in liquid Ga, and then GaSe crystals precipitate and grow on the liquid Ga surface. (b) Optical images of (I) GaSe in liquid Ga and (II) stripped down, and (III) SEM image of crystals, showing the triangle morphology and smooth surface. (c) High resolution TEM (HRTEM) image of the GaSe crystal. The inset selected area electron diffraction (SAED) pattern shows a single-crystalline structure. (d) Schemes of the atomic structure of GaSe viewed from top and side. Reprinted with permission.[131] Copyright (2021), Tsinghua University Press and Springer-Verlag GmbH, Germany, part of Springer Nature.

nolysis of Ga_2O_3 and In_2O_3 as precursors, with InN requiring an extra bromination step, creates 2D GaN and InN nanosheets.[128] The resultant 2D GaN films are utilized to construct patterned GaN-based photodetector arrays through vdW transfer, UV lithography patterning and Ti/Au thermal evaporation.[129] Electrochemical substitution represents another notable technique for synthesizing 2D materials using LM reactors, which leverages the dynamic EDL of LMs. For instance, an aqueous solution of the $(NH_4)_2MoS_4$ precursor reduced on the EGaIn surface produces expansive planar MoS_2 with an oxide-free EGaIn interface acting as both a reduction agent and a template.[18]

Moreover, LMs in their molten state exhibit an amorphous and isotropic atomic structure, which helps in mitigating the negative effects typically associated with grain boundaries. The increased mobility of atoms and electrons in the liquid phase promotes the spontaneous assembly of 2D materials on the LM surface. When the LM is subsequently solidified, this process triggers the self-limited growth of 2D materials, resulting in the attainment of a strictly uniform monolayer. The unique shear transformation of LMs facilitates the ultraclean sliding transfer process of the deposited planar materials on the LM interface.[19] For instance, 2D layered chalcogenide crystals, such as GaSe and $Ga_xIn_{1-x}Se$, have been achieved using Ga or EGaIn through low-temperature vapor-phase growth.[130] Alternatively, centimeter-size GaSe crystals were prepared through atmospheric pressure CVD in liquid Ga-assisted synthesis at a higher temperature (Fig. 12a) After removal from the synthesis boat, large-scale GaSe nanosheets with a smooth surface, a single-crystalline structure and high quality were obtained (Fig. 12b–d).[131]

3.2.3 2D graphitic materials. Additionally, the atomically smooth and unpolarized surface of LMs not only aids in the deposition of planar materials like graphene oxide (GO), but also enhances the ultra-clean slide transfer processes. The super-reactive interface of LMs, abundant with free electrons and off-domain ions, is effective for room-temperature reduction of GO films. For instance, free-standing composites of LM-reduced graphene oxide (LM@rGO) nanosheets were synthesized by immersing a Si/SiO_2 substrate coated with GO

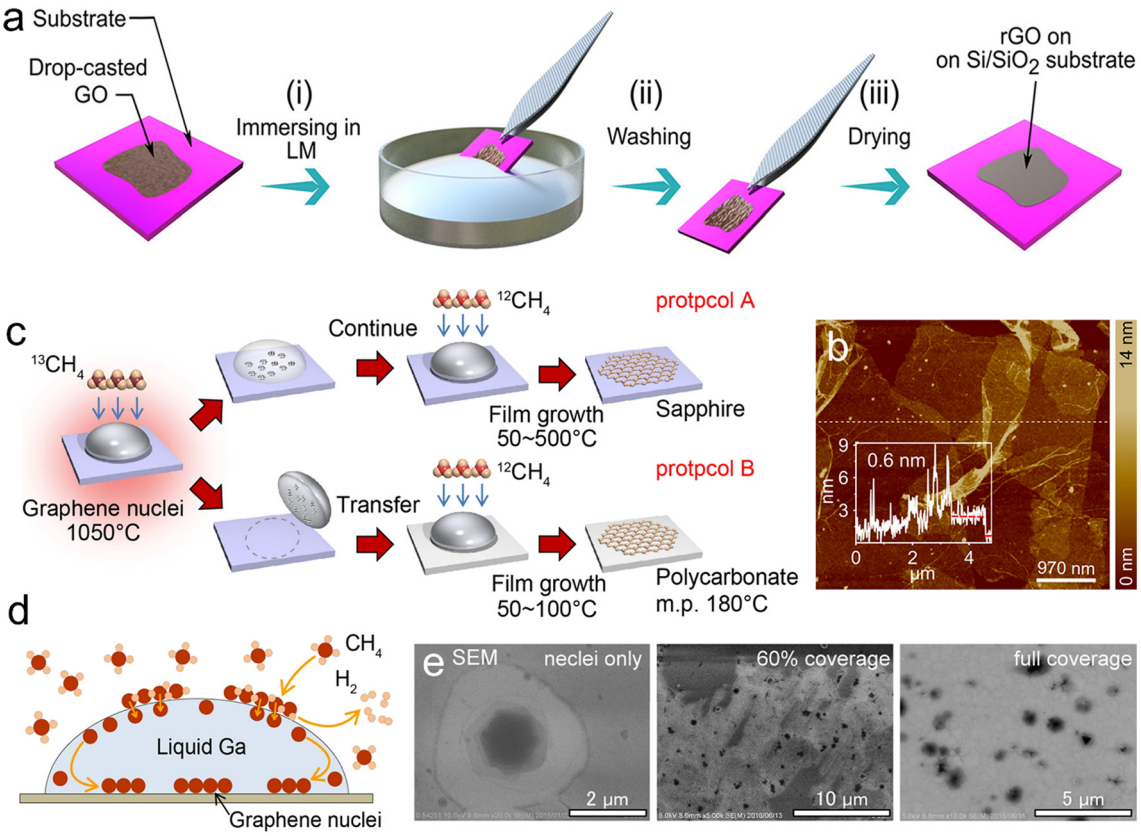

Fig. 13 Liquid Ga for the synthesis of graphene 2D materials. (a) Schematic representation of a GO layer immobilized on a Si/SiO_2 substrate reduced by liquid Ga. (b) AFM images and the thickness profile of the rGO sample showing a monolayer rGO sheet with a thickness of 0.6 nm. Reprinted with permission.[19] Copyright (2021), American Chemical Society. (c) Schematic diagrams of two methods (A, continuous and B, stepwise) for graphene edge growth using liquid Ga. The process involves the formation of graphene nuclei using ^{13}C CH_4 at 1050 °C for 300 s and graphene edge growth with $^{12}CH_4$ at a lower temperature. (d) Mechanism of graphene nuclei generation and film growth. (e) SEM images of graphene grown at 100 °C with different coverage; 0% (^{13}C nuclei only), 60% (partly covered) and 100% (full coverage). After the high-temperature growth of GO nuclei with ^{13}C-CH_4 and further low-temperature growth with ^{12}C-CH_4, the product still contains only ^{13}C. Reprinted with permission.[132] Copyright (2017), Springer Nature.

flakes in EGaIn. In this process, the LM acts as an ultra-smooth soft reaction template to reduce graphene oxide (Fig. 13a and b).[19] Alternatively, core–shell structured LM@rGO nanoparticles were prepared *via* a sonochemical method, in which Ga provides electrons for the redox reactions as a strong reducing substance. Moreover, the partial electric field produced by the electron transfer assists in the self-assembly of rGO onto the LM droplet surface.[29]

Liquid metals not only serve as a common interface for the retention and generation of planar materials, but they also exhibit a natural catalytic effect, particularly effective in breaking C–O, C–N and C–H bonds in organic molecules and reconstructing them as graphitic C–C bonds at room temperature. Ga-based LMs, doped with metals such as In and Sn, are especially conducive to dissociating organic precursors to form free radicals for adsorption. Upon leveraging this capability, a wide range of carbon-containing sheets can be fabricated, ranging from graphene-like planar surfaces to highly porous 2D graphitic material sheets, in both monolayers and multilayers.[133] A practical application of this is the continuous production of high-quality GO sheets using liquid Ga as a catalyst and diluted $^{13}C/^{12}C$ methane as the CVD source gas (Fig. 13c–e). These Ga catalysts facilitate catalytic conversion on various substrates, such as sapphire or plastic polycarbonate, at a temperature near room temperature.[132]

3.3 Metal–organic frameworks

Metal–organic frameworks (MOFs) represent a category of porous polymeric materials, wherein metal ions are interconnected by organic bridging ligands.[134] MOFs have attracted wide interest in the fields of energy storage,[135] small molecule detection,[136] optical sensors,[137] catalysis,[138] and electromagnetic wave absorption due to their excellent properties such as high internal surface area, tunable pore size, ordered crystal structure, and excellent chemical stability.[136,139] Ga-based LMs have demonstrated impressive capabilities as fluid electrodes in the electrochemical synthesis of MOFs. These Ga-based LMs act as activators, accelerating electrosynthesis and enabling reactions at lower onset potentials. Moreover, when submerged in an electrolyte solution, solute metals in the Ga-based LMs dynamically migrate and accumulate at the interface, enhancing electrode interfacial exposure and boosting the reaction efficiency (Fig. 14a).[140] Additionally, the electrification of LMs induces interfacial Marangoni flow, facilitating the continuous progression of chemical reactions through releasing adhered reaction products from the electrode surface

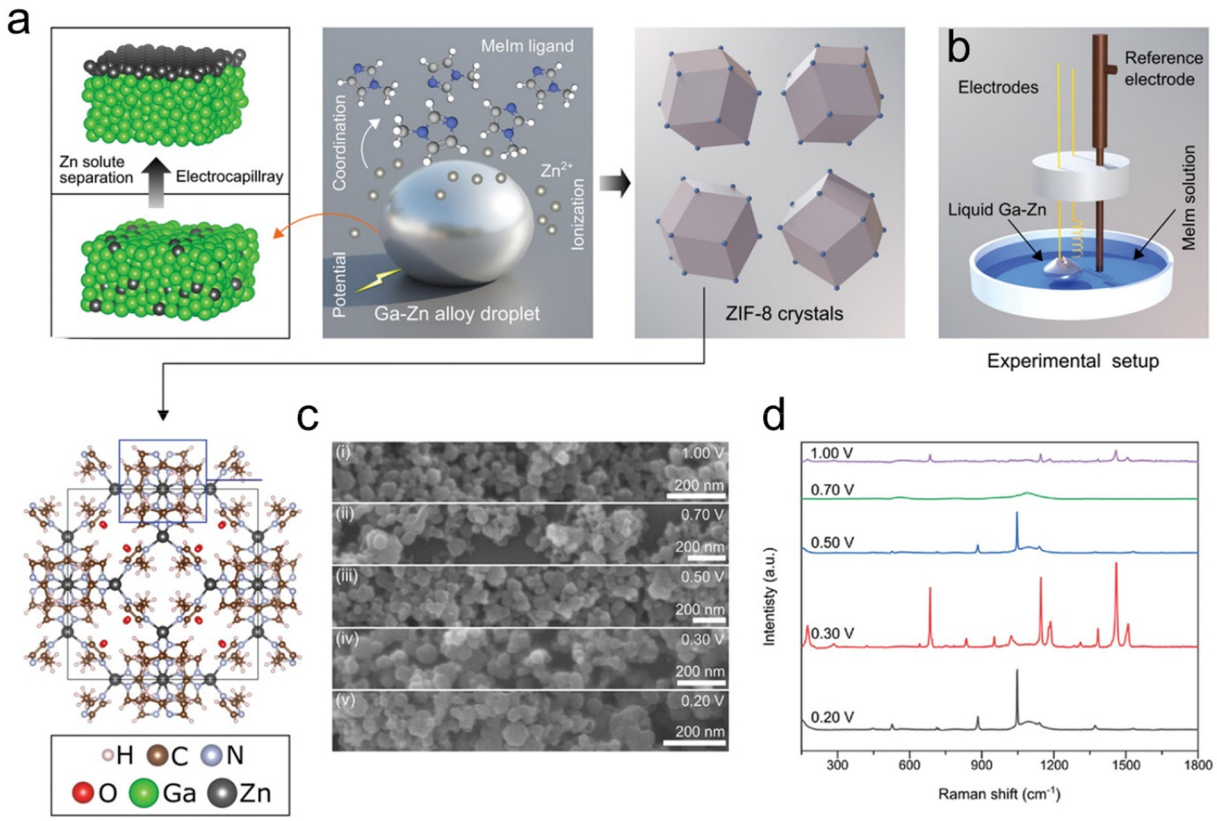

Fig. 14 GaZn alloys for the synthesis of ZIF-8. (a) Schematic diagram of the electrosynthesis of ZIF-8. The solute metal Zn in GaZn alloys migrates to the surface and is ionized into Zn^{2+}, which coordinates with deprotonated organic linkers to form the polyhedral ZIF-8. (b) The setup of the three-electrode cell, in which a Ga–Zn alloy was used as an anode for the electrosynthesis of ZIF-8. (c) SEM images of products synthesized at different voltages showing a rhombic polyhedral geometry. (i) 0.20 V; (ii) 0.30 V; (iii) 0.50 V; (iv) 0.70 V; (v) 1.00 V *versus* SCE, respectively. (d) Raman spectra of products synthesized at different voltages. The curve corresponding to 0.3 V shows all the characteristic peaks of ZIF-8, which indicates the successful synthesis of ZIF-8. Reprinted with permission.[141] Copyright (2023), Wiley-VCH.

to enhance the overall efficiency and effectiveness of the electrochemical synthesis (Fig. 14b).[141] Notable examples of this application include the production of layered Zn-MOFs using a liquid Ga–Zn alloy as the working electrode[26] as well as synthesizing zeolitic imidazolate frameworks (ZIFs)-8 through anodic oxidation of a Ga–Zn liquid alloy (Fig. 14c and d).[141]

4 Challenges and opportunities

Although there have been notable achievements in utilizing Ga-based LMs as solvents or reaction media for preparing various functional materials, this research area remains largely exploratory with vast untapped potential. This review identifies key challenges and promising directions for future research on LM reactors, aiming to stimulate further investigation in this area. The primary considerations can be outlined as follows:

(1) Ga-based liquid metal solvents offer the ability to dissolve various metal elements, creating alloys that blend the advantages of each component. Future research interest has surged in exploring the doping of Ga-based metal alloys with different components and ratios to produce a range of functional alloys, such as corrosion resistance, magnetism, high strength, flexibility, shape memory, elastocaloric properties, *etc*.

(2) The sonochemical-assisted GRR strategy, relying on Ga, can be used to fabricate metal nanocrystals, multi-alloyed NPs and core–shell structure NPs. However, the nanostructures generated through electrocoupling substitution and sonication processes exhibit stochastic characteristics, leading to uncertainties in dimensions, elemental distributions, and morphologies.[59] This lack of control limits the application of uniform and specific nanostructured NPs. Therefore, further research should focus on precisely regulating the NP structure.

(3) Nanoporous metals' properties can be significantly affected by the challenge of precisely controlling the residual content of sub-inert metals.[142] Furthermore, the microstructure of stabilized nanoporous metals is essential for their applications in catalysts, sensing, and other areas. These two aspects are also significant considerations in Ga solvent-based dealloying strategies.

(4) HEA NPs can be synthesized by a variety of methods, such as carbothermal shock synthesis, mechanical alloying, microwave heating, wet chemistry, liquid laser ablation, chemical dealloying, *etc*.[143] However, these methods always require the application of extreme heating temperatures to provide high mixing entropy.[82] The easy alloying property of liquid Ga makes it possible to synthesize HEA NPs at low temperatures. Future investigations could focus on the utilization of liquid Ga in diverse synthesis techniques for HEA NPs, aiming to uncover more efficient, gentle and cost-effective methods for HEA NP synthesis.

(5) The fluid-like, ultra-smooth surfaces of Ga-based LMs are extensively used in synthesizing 2D materials. Yet, an underexplored aspect is their short-range atomic "layer" surface in the near-surface region. Current research lacks evidence of the specific impact of this near-surface atomic layering on materials synthesis in Ga-based LM systems. Future studies could focus more on how liquid Ga's layered surfaces influence the interfacial growth of crystals and 2D materials.

(6) Single atom (SA) catalysts are prized for their maximum atom utilization and high catalytic selectivity. Common SA preparation processes, such as atomic deposition and wet chemistry, often demand harsh conditions (such as high temperatures, high pressures, strong acids or tedious procedures), while the solute elements in Ga-based metal alloy catalysts are mobile and atomically separated. Those solute elements resemble single atoms, and the solvent Ga effectively prevents bonding between solute elements, suggesting the possibility of producing metal SAs under milder conditions, which could facilitate large-scale production of SA catalysts. There is considerable potential in using Ga-based solvents for producing SA catalysts for a wide range of applications. Also, Ga SAs have been less explored so far, and Ga's fluxional nature at the single atomic level and the corresponding catalytic mechanism due to inherent mobility require deeper investigation.

(7) In synthesizing 2D metal oxides, the strategies utilizing LMs' self-limiting oxidation combined with subsequent transfer stripping techniques offer compelling advantages. However, two key areas need further optimization. Firstly, achieving complete, single-attempt delamination of all 2D metal oxides presents a challenge. Imperfect contact between the substrate and the LM surface, along with inconsistent application of contact force, can lead to the rupture of the oxide layer or restrict the size of the 2D metal oxide. Secondly, issues with substrate bonding or uneven force application can result in residual LM being left on the substrate. This is a significant hurdle in the fabrication of high-purity and high-precision electronic devices.

(8) Currently, the exploration of MOF production using LM reactors is in its early stages, primarily focusing on Zn-based ZIFs. Considering LMs' capability to alloy with various metal elements and the potential universal applicability of the electrochemical synthesis method discussed in this review, future research could pivot towards electrochemically synthesizing a diverse range of metal-based MOFs using Ga–X alloys as anodes (where 'X' represents other metal elements). Such an efficient production method might have the potential to significantly expand the use of MOF materials, especially if the range of metal elements in LM-based MOF systems can be broadened.

5 Conclusion

Ga-based room temperature LMs possess a wonderful combination of metallic and liquid solvent features, including high metal solubility, low standard reduction potential, self-limiting oxidation, and ultra-smooth surfaces. This unique combination positions Ga-based LMs as exceptional reaction media for the exploration and fabrication of a diverse range of nanomaterials. In this review, we summarize the recent develop-

ments for the fabrication of pure metallic materials (metal alloys, metal crystals, porous metals, high-entropy alloys and metallic single atoms), metal–inorganic compounds (2D metal oxides, 2D metallic inorganic compounds and 2D graphitic materials), and metal–organic composites (metal–organic frameworks) from liquid Ga reactors.

Looking forward, the potential applications and innovations in nanomaterial synthesis using Ga-based LMs are vast and largely untapped. As researchers continue to unravel the complexities and capabilities of these fascinating materials, we anticipate a surge in groundbreaking discoveries and applications across various fields, including electronics, catalysis, energy storage, and environmental technology. The versatility and unique properties of Ga-based LMs are poised to play a pivotal role in the future of materials science, paving the way for more efficient, sustainable, and innovative technological solutions.

Author contributions

Ming Wang: writing – original draft and review and editing. Yiliang Lin: supervision, writing – original draft, and review and editing.

Conflicts of interest

The authors declare no conflict of interest.

Acknowledgements

The authors are grateful for the financial support from the NUS Start-up Grant for this work.

References

1 Q. Wang, Y. Yu and J. Liu, *Adv. Eng. Mater.*, 2018, **20**, 1700781.
2 F.-M. Allioux, M. B. Ghasemian, W. Xie, A. P. O'Mullane, T. Daeneke, M. D. Dickey and K. Kalantar-Zadeh, *Nanoscale Horiz.*, 2022, **7**, 141–167.
3 M. J. Regan, E. H. Kawamoto, S. Lee, P. S. Pershan, N. Maskil, M. Deutsch, O. M. Magnussen, B. M. Ocko and L. E. Berman, *Phys. Rev. Lett.*, 1995, **75**, 2498–2501.
4 T. Daeneke, K. Khoshmanesh, N. Mahmood, I. A. de Castro, D. Esrafilzadeh, S. J. Barrow, M. D. Dickey and K. Kalantar-zadeh, *Chem. Soc. Rev.*, 2018, **47**, 4073–4111.
5 S.-Y. Tang, C. Tabor, K. Kalantar-Zadeh and M. D. Dickey, *Annu. Rev. Mater. Res.*, 2021, **51**, 381–408.
6 C. A. Echeverria, J. Tang, Z. Cao, D. Esrafilzadeh and K. Kalantar-Zadeh, *ACS Appl. Nano Mater.*, 2022, **5**, 6820–6831.
7 S. Chen, H.-Z. Wang, R.-Q. Zhao, W. Rao and J. Liu, *Matter*, 2020, **2**, 1446–1480.
8 M. Baharfar, J. Zheng, R. Abbasi, S. Lim, V. Kundi, P. V. Kumar, Md. A. Rahim, C. Zhang, K. Kalantar-Zadeh and M. Mayyas, *Chem. Mater.*, 2022, **34**, 10761–10771.
9 S. A. Idrus-Saidi, J. Tang, S. Lambie, J. Han, M. Mayyas, M. B. Ghasemian, F.-M. Allioux, S. Cai, P. Koshy and P. Mostaghimi, *Science*, 2022, **378**, 1118–1124.
10 H. Liu, K. Wang, K. E. Aasmundtveit and N. Hoivik, *J. Electron. Mater.*, 2012, **41**, 2453–2462.
11 Y. Chi, P. V. Kumar, J. Zheng, C. Kong, R. Yu, L. Johnston, M. B. Ghasemian, Md. A. Rahim, T. Kumeria, D. Chu, X. Lu, G. Mao, K. Kalantar-Zadeh and J. Tang, *ACS Nano*, 2023, **17**, 17070–17081.
12 M. B. Ghasemian, M. Mayyas, S. A. Idrus-Saidi, M. A. Jamal, J. Yang, S. S. Mofarah, E. Adabifiroozjaei, J. Tang, N. Syed, A. P. O'Mullane, T. Daeneke and K. Kalantar-Zadeh, *Adv. Funct. Mater.*, 2019, **29**, 1901649.
13 M. K. Akbari, Z. Hai, Z. Wei, R. K. Ramachandran, C. Detavernier, M. Patel, J. Kim, F. Verpoort, H. Lu and S. Zhuiykov, *J. Mater. Chem. C*, 2019, **7**, 5584–5595.
14 H. Li, R. Abbasi, Y. Wang, F. M. Allioux, P. Koshy, S. A. Idrus-Saidi, M. A. Rahim, J. Yang, M. Mousavi, J. Tang, M. B. Ghasemian, R. Jalili, K. Kalantar-Zadeh and M. Mayyas, *J. Mater. Chem. C*, 2020, **8**, 1656–1665.
15 L. Duan, T. Zhou, Y. Zhang, J. Zhao, H. Zheng, B. Zi, J. Zhang, Q. Li, J. Liu and Q. Liu, *Adv. Mater.*, 2023, **35**, 2210515.
16 A. Goff, P. Aukarasereenont, C. K. Nguyen, R. Grant, N. Syed, A. Zavabeti, A. Elbourne and T. Daeneke, *Dalton Trans.*, 2021, **50**, 7513–7526.
17 P. Aukarasereenont, A. Goff, C. K. Nguyen, C. F. McConville, A. Elbourne, A. Zavabeti and T. Daeneke, *Chem. Soc. Rev.*, 2022, **51**, 1253–1276.
18 Y. Wang, M. Mayyas, J. Yang, J. Tang, M. B. Ghasemian, J. Han, A. Elbourne, T. Daeneke, R. B. Kaner and K. Kalantar-Zadeh, *Adv. Funct. Mater.*, 2021, **31**, 2005866.
19 M. Baharfar, M. Mayyas, M. Rahbar, F.-M. Allioux, J. Tang, Y. Wang, Z. Cao, F. Centurion, R. Jalili, G. Liu and K. Kalantar-Zadeh, *ACS Nano*, 2021, **15**, 19661–19671.
20 M. K. Sunkara, S. Sharma, R. Miranda, G. Lian and E. C. Dickey, *Appl. Phys. Lett.*, 2001, **79**, 1546–1548.
21 S. Zhao, J. Zhang and L. Fu, *Adv. Mater.*, 2021, **33**, 2005544.
22 Y. Ding, M. Zeng and L. Fu, *Matter*, 2019, **1**, 1099–1103.
23 K. Y. Kwon, S. Cheeseman, A. Frias-De-Diego, H. Hong, J. Yang, W. Jung, H. Yin, B. J. Murdoch, F. Scholle, N. Crook, E. Crisci, M. D. Dickey, V. K. Truong and T. Kim, *Adv. Mater.*, 2021, **33**, 2104298.
24 J.-H. Fu, T.-Y. Liu, Y. Cui and J. Liu, *Adv. Mater. Interfaces*, 2021, **8**, 2001936.
25 E. A. Sharova, A. S. Falchevskaya, S. S. Leonchuk, A. V. Redkov, V. Nikolaev and V. V. Vinogradov, *Chem. Commun.*, 2023, **59**, 10928–10931.
26 J. Zheng, M. Mousavi, M. Baharfar, A. Sharma, T. Kumeria, J. Han, P. Kumar, K. Kalantar-Zadeh and M. Mayyas, *J. Mater. Chem. C*, 2022, **10**, 14963–14970.

27 A. S. Falchevskaya, A. Y. Prilepskii, S. A. Tsvetikova, E. I. Koshel and V. V. Vinogradov, *Chem. Mater.*, 2021, **33**, 1571–1580.
28 A. Jannat, Q. Yao, A. Zavabeti, N. Syed, B. Y. Zhang, T. Ahmed, S. Kuriakose, M. Mohiuddin, N. Pillai, F. Haque, G. Ren, D. M. Zhu, N. Cheng, Y. Du, S. A. Tawfik, M. J. S. Spencer, B. J. Murdoch, L. Wang, C. F. McConville, S. Walia, T. Daeneke, L. Zhu and J. Z. Ou, *Mater. Horiz.*, 2020, **7**, 827–834.
29 Y. Wang, S. Wang, H. Chang and W. Rao, *Adv. Mater. Interfaces*, 2020, **7**, 2000626.
30 M. J. Regan, H. Tostmann, P. S. Pershan, O. M. Magnussen, E. DiMasi, B. M. Ocko and M. Deutsch, *Phys. Rev. B: Condens. Matter Mater. Phys.*, 1997, **55**, 10786–10790.
31 N. Cabrera and N. F. Mott, *Rep. Prog. Phys.*, 1949, **12**, 163.
32 M. J. Regan, P. S. Pershan, O. M. Magnussen, B. M. Ocko, M. Deutsch and L. E. Berman, *Phys. Rev. B: Condens. Matter Mater. Phys.*, 1997, **55**, 15874–15884.
33 Y. Lin, C. Cooper, M. Wang, J. J. Adams, J. Genzer and M. D. Dickey, *Small*, 2015, **11**, 6397–6403.
34 R. N. S. Sodhi, P. Brodersen, L. Cademartiri, M. M. Thuo and C. A. Nijhuis, *Surf. Interface Anal.*, 2017, **49**, 1309–1315.
35 A. Zavabeti, J. Z. Ou, B. J. Carey, N. Syed, R. Orrell-Trigg, E. L. Mayes, C. Xu, O. Kavehei, A. P. O'Mullane and R. B. Kaner, *Science*, 2017, **358**, 332–335.
36 W. Babatain, M. S. Kim and M. M. Hussain, *Adv. Funct. Mater.*, 2023, 2308116.
37 R. S. Datta, N. Syed, A. Zavabeti, A. Jannat, M. Mohiuddin, M. Rokunuzzaman, B. Y. Zhang, M. A. Rahman, P. Atkin, K. A. Messalea, M. B. Ghasemian, E. D. Gaspera, S. Bhattacharyya, M. S. Fuhrer, S. P. Russo, C. F. McConville, D. Esrafilzadeh, K. Kalantar-Zadeh and T. Daeneke, *Nat. Electron.*, 2020, **3**, 51–58.
38 L. Chen, Z. Kong, S. Yue, J. Liu, J. Deng, Y. Xiao, R. G. Mendes, M. H. Rümmeli, L. Peng and L. Fu, *Chem. Mater.*, 2015, **27**, 8230–8236.
39 O. G. Shpyrko, R. Streitel, V. S. K. Balagurusamy, A. Y. Grigoriev, M. Deutsch, B. M. Ocko, M. Meron, B. Lin and P. S. Pershan, *Science*, 2006, **313**, 77–80.
40 K. Kalantar-Zadeh, J. Tang, T. Daeneke, A. P. O'Mullane, L. A. Stewart, J. Liu, C. Majidi, R. S. Ruoff, P. S. Weiss and M. D. Dickey, *ACS Nano*, 2019, **13**, 7388–7395.
41 M. G. Kanatzidis, R. Pöttgen and W. Jeitschko, *Angew. Chem., Int. Ed.*, 2005, **44**, 6996–7023.
42 A. Turchanin and W. Freyland, *Chem. Phys. Lett.*, 2004, **387**, 106–109.
43 I. S. Golovin, *Materials*, 2023, **16**, 2365.
44 A. P. Rao, M. T. Cook, H. L. Hall and M. B. Shattan, *Atoms*, 2019, **7**, 84.
45 J. Li, Z. Chen, J. Jing and J. Hou, *J. Mater. Sci. Technol.*, 2020, **41**, 33–42.
46 T. Itami, R. Xu and W. van der Lugt, *J. Alloys Compd.*, 1993, **201**, 37–41.
47 Z. Yao, X. Tian, L. Jiang, H. Hao, G. Zhang, S. Wu, Z. Zhao and N. Gerile, *J. Alloys Compd.*, 2015, **637**, 431–435.
48 M. M. Yazdanpanah, S. A. Harfenist, A. Safir and R. W. Cohn, *J. Appl. Phys.*, 2005, **98**, 073510.
49 J. Tang, J. Tang, M. Mayyas, M. B. Ghasemian, J. Sun, M. A. Rahim, J. Yang, J. Han, D. J. Lawes, R. Jalili, T. Daeneke, M. G. Saborio, Z. Cao, C. A. Echeverria, F.-M. Allioux, A. Zavabeti, J. Hamilton, V. Mitchell, A. P. O'Mullane, R. B. Kaner, D. Esrafilzadeh, M. D. Dickey and K. Kalantar-Zadeh, *Adv. Mater.*, 2022, **34**, 2105789.
50 N. R. Wood, A. I. Wolsiefer, R. W. Cohn and S. J. Williams, *Electrophoresis*, 2013, **34**, 1922–1930.
51 M. A. H. Khondoker and D. Sameoto, *Smart Mater. Struct.*, 2016, **25**, 093001.
52 D. Wang, J. Ye, Y. Bai, F. Yang, J. Zhang, W. Rao and J. Liu, *Adv. Mater.*, 2023, 2303533.
53 L. Wang and J. Liu, *Front. Energy*, 2013, **7**, 317–332.
54 H. Okamoto, *J. Phase Equilib. Diffus.*, 2016, **37**, 350–362.
55 O. Oloye, C. Tang, A. Du, G. Will and A. P. O'Mullane, *Nanoscale*, 2019, **11**, 9705–9715.
56 L. Castilla-Amorós, D. Stoian, J. R. Pankhurst, S. B. Varandili and R. Buonsanti, *J. Am. Chem. Soc.*, 2020, **142**, 19283–19290.
57 F. Hoshyargar, J. Crawford and A. P. O'Mullane, *J. Am. Chem. Soc.*, 2017, **139**, 1464–1471.
58 L. Ren, N. Cheng, X. Man, D. Qi, Y. Liu, G. Xu, D. Cui, N. Liu, J. Zhong, G. Peleckis, X. Xu, S. X. Dou and Y. Du, *Adv. Mater.*, 2021, **33**, 2008024.
59 H. Lu, S.-Y. Tang, J. Zhu, X. Huang, H. Forgham, X. Li, A. Shen, G. Yun, J. Hu, S. Zhang, T. P. Davis, W. Li and R. Qiao, *Adv. Funct. Mater.*, 2024, **34**, 2311300.
60 N. Taccardi, M. Grabau, J. Debuschewitz, M. Distaso, M. Brandl, R. Hock, F. Maier, C. Papp, J. Erhard, C. Neiss, W. Peukert, A. Görling, H.-P. Steinrück and P. Wasserscheid, *Nat. Chem.*, 2017, **9**, 862–867.
61 D. Esrafilzadeh, A. Zavabeti, R. Jalili, P. Atkin, J. Choi, B. J. Carey, R. Brkljača, A. P. O'Mullane, M. D. Dickey, D. L. Officer, D. R. MacFarlane, T. Daeneke and K. Kalantar-Zadeh, *Nat. Commun.*, 2019, **10**, 865.
62 W. Zhu, Z. Chen, Y. Pan, R. Dai, Y. Wu, Z. Zhuang, D. Wang, Q. Peng, C. Chen and Y. Li, *Adv. Mater.*, 2019, **31**, 1800426.
63 B. Li and H. C. Zeng, *Adv. Mater.*, 2019, **31**, 1801104.
64 L. Wang, J. Wan, J. Wang and D. Wang, *Small Struct.*, 2021, **2**, 2000041.
65 E. Yasun, S. Gandhi, S. Choudhury, R. Mohammadinejad, F. Benyettou, N. Gozubenli and H. Arami, *J. Drug Delivery Sci. Technol.*, 2020, **60**, 102094.
66 Z. Weng, W. Liu, L.-C. Yin, R. Fang, M. Li, E. I. Altman, Q. Fan, F. Li, H.-M. Cheng and H. Wang, *Nano Lett.*, 2015, **15**, 7704–7710.
67 R. Lin, E. Hu, M. Liu, Y. Wang, H. Cheng, J. Wu, J.-C. Zheng, Q. Wu, S. Bak, X. Tong, R. Zhang, W. Yang, K. A. Persson, X. Yu, X.-Q. Yang and H. L. Xin, *Nat. Commun.*, 2019, **10**, 1650.

68 F. Lin, D. Nordlund, Y. Li, M. K. Quan, L. Cheng, T.-C. Weng, Y. Liu, H. L. Xin and M. M. Doeff, *Nat. Energy*, 2016, **1**, 1–8.
69 J.-C. Shao and H.-J. Jin, *J. Mater. Sci.*, 2020, **55**, 8337–8345.
70 Y. Zhang, Q. Bai, W. Yang and Z. Zhang, *Sci. China: Technol. Sci.*, 2021, **64**, 2229–2236.
71 X. Guo, C. Zhang, Q. Tian and D. Yu, *Mater. Today Commun.*, 2021, **26**, 102007.
72 A. Wittstock, V. Zielasek, J. Biener, C. M. Friend and M. Bäumer, *Science*, 2010, **327**, 319–322.
73 J. Biener, A. Wittstock, L. A. Zepeda-Ruiz, M. M. Biener, V. Zielasek, D. Kramer, R. N. Viswanath, J. Weissmüller, M. Bäumer and A. V. Hamza, *Nat. Mater.*, 2009, **8**, 47–51.
74 H.-J. Qiu, X. Li, H.-T. Xu, H.-J. Zhang and Y. Wang, *J. Mater. Chem. C*, 2014, **2**, 9788–9799.
75 J. T. Zhang and C. M. Li, *Chem. Soc. Rev.*, 2012, **41**, 7016–7031.
76 W. Yuan, Y. Tang, X. Yang and Z. Wan, *Appl. Energy*, 2012, **94**, 309–329.
77 Y. Zhang, X. Yang and P. K. Liaw, *JOM*, 2012, **64**, 830–838.
78 S. H. Shim, H. Pouraliakbar and S. I. Hong, *Mater. Sci. Eng.*, 2021, **825**, 141875.
79 W.-Y. Ching, S. San, J. Brechtl, R. Sakidja, M. Zhang and P. K. Liaw, *npj Comput. Mater.*, 2020, **6**, 1–10.
80 A. Takeuchi and A. Inoue, *Mater. Trans.*, 2005, **46**, 2817–2829.
81 J. Bai, X. Jin, H. Yang and J. Qiao, *J. Alloys Compd.*, 2022, **919**, 165736.
82 G. Cao, J. Liang, Z. Guo, K. Yang, G. Wang, H. Wang, X. Wan, Z. Li, Y. Bai, Y. Zhang, J. Liu, Y. Feng, Z. Zheng, C. Lu, G. He, Z. Xiong, Z. Liu, S. Chen, Y. Guo, M. Zeng, J. Lin and L. Fu, *Nature*, 2023, **619**, 73–77.
83 Y. Yao, Z. Huang, P. Xie, S. D. Lacey, R. J. Jacob, H. Xie, F. Chen, A. Nie, T. Pu, M. Rehwoldt, D. Yu, M. R. Zachariah, C. Wang, R. Shahbazian-Yassar, J. Li and L. Hu, *Science*, 2018, **359**, 1489–1494.
84 P. Xie, Y. Yao, Z. Huang, Z. Liu, J. Zhang, T. Li, G. Wang, R. Shahbazian-Yassar, L. Hu and C. Wang, *Nat. Commun.*, 2019, **10**, 4011.
85 S. Gao, S. Hao, Z. Huang, Y. Yuan, S. Han, L. Lei, X. Zhang, R. Shahbazian-Yassar and J. Lu, *Nat. Commun.*, 2020, **11**, 2016.
86 N. A. Frey, S. Peng, K. Cheng and S. Sun, *Chem. Soc. Rev.*, 2009, **38**, 2532–2542.
87 M. B. Cortie and A. M. McDonagh, *Chem. Rev.*, 2011, **111**, 3713–3735.
88 Q. Sun, N. Wang, T. Zhang, R. Bai, A. Mayoral, P. Zhang, Q. Zhang, O. Terasaki and J. Yu, *Angew. Chem., Int. Ed.*, 2019, **58**, 18570–18576.
89 L. Peng, L. Shang, T. Zhang and G. I. N. Waterhouse, *Adv. Energy Mater.*, 2020, **10**, 2003018.
90 X.-F. Yang, A. Wang, B. Qiao, J. Li, J. Liu and T. Zhang, *Acc. Chem. Res.*, 2013, **46**, 1740–1748.
91 Y. Lin, X. Gao, J. Yue, Y. Fang, J. Shi, L. Meng, C. Clayton, X.-X. Zhang, F. Shi and J. Deng, *Nat. Chem.*, 2023, **15**, 119–128.
92 M. Zhang, W. Xu, C.-L. Ma, J. Yu, Y.-T. Liu and B. Ding, *ACS Nano*, 2022, **16**, 4186–4196.
93 L. Wu, J. Xin, Y. Wang, K. Zhang, J. Zhang, J. Sun, R. Zou and J. Liang, *J. Energy Chem.*, 2023, **84**, 363–373.
94 Z. Zhang, J. Zhu, S. Chen, W. Sun and D. Wang, *Angew. Chem., Int. Ed.*, 2023, **62**, e202215136.
95 M. A. Rahim, J. Tang, A. J. Christofferson, P. V. Kumar, N. Meftahi, F. Centurion, Z. Cao, J. Tang, M. Baharfar and M. Mayyas, *Nat. Chem.*, 2022, **14**, 935–941.
96 J. Tang, A. J. Christofferson, J. Sun, Q. Zhai, P. V. Kumar, J. A. Yuwono, M. Tajik, N. Meftahi, J. Tang, L. Dai, G. Mao, S. P. Russo, R. B. Kaner, M. A. Rahim and K. Kalantar-Zadeh, *Nat. Nanotechnol.*, 2023, 1–5.
97 M. Kettner, S. Maisel, C. Stumm, M. Schwarz, C. Schuschke, A. Görling and J. Libuda, *J. Catal.*, 2019, **369**, 33–46.
98 Y. Qi, N. Li, K. Zhang, Y. Yang, Z. Ren, J. You, Q. Hou, C. Shen, T. Jin and Z. Peng, *Adv. Mater.*, 2022, **34**, 2204810.
99 T. Liu, P. Sen and C.-J. Kim, *J. Microelectromech. Syst.*, 2012, **21**, 443–450.
100 M. D. Dickey, R. C. Chiechi, R. J. Larsen, E. A. Weiss, D. A. Weitz and G. M. Whitesides, *Adv. Funct. Mater.*, 2008, **18**, 1097–1104.
101 Z. J. Farrell and C. Tabor, *Langmuir*, 2018, **34**, 234–240.
102 M. Li, L. Li, Y. Fan, L. Huang, D. Geng and W. Yang, *Nanoscale Adv.*, 2021, **3**, 4411–4415.
103 N. Syed, A. Zavabeti, J. Z. Ou, M. Mohiuddin, N. Pillai, B. J. Carey, B. Y. Zhang, R. S. Datta, A. Jannat, F. Haque, K. A. Messalea, C. Xu, S. P. Russo, C. F. McConville, T. Daeneke and K. Kalantar-Zadeh, *Nat. Commun.*, 2018, **9**, 3618.
104 T. Daeneke, P. Atkin, R. Orrell-Trigg, A. Zavabeti, T. Ahmed, S. Walia, M. Liu, Y. Tachibana, M. Javaid, A. D. Greentree, S. P. Russo, R. B. Kaner and K. Kalantar-Zadeh, *ACS Nano*, 2017, **11**, 10974–10983.
105 R. C. Chiechi, E. A. Weiss, M. D. Dickey and G. M. Whitesides, *Angew. Chem., Int. Ed.*, 2008, **47**, 142–144.
106 M. B. Ghasemian, A. Zavabeti, M. Mousavi, B. J. Murdoch, A. J. Christofferson, N. Meftahi, J. Tang, J. Han, R. Jalili, F.-M. Allioux, M. Mayyas, Z. Chen, A. Elbourne, C. F. McConville, S. P. Russo, S. Ringer and K. Kalantar-Zadeh, *Adv. Mater.*, 2021, **33**, 2104793.
107 K. A. Messalea, N. Syed, A. Zavabeti, M. Mohiuddin, A. Jannat, P. Aukarasereenont, C. K. Nguyen, M. X. Low, S. Walia, B. Haas, C. T. Koch, N. Mahmood, K. Khoshmanesh, K. Kalantar-Zadeh and T. Daeneke, *ACS Nano*, 2021, **15**, 16067–16075.
108 A. Martin, W. Kiarie, B. Chang and M. Thuo, *Angew. Chem., Int. Ed.*, 2020, **59**, 352–357.
109 A. Martin, C. Du, B. Chang and M. Thuo, *Chem. Mater.*, 2020, **32**, 9045–9055.
110 M. A. Creighton, M. C. Yuen, M. A. Susner, Z. Farrell, B. Maruyama and C. E. Tabor, *Langmuir*, 2020, **36**, 12933–12941.

111 A. Zavabeti, B. Y. Zhang, I. A. de Castro, J. Z. Ou, B. J. Carey, M. Mohiuddin, RobiS. Datta, C. Xu, A. P. Mouritz, C. F. McConville, A. P. O'Mullane, T. Daeneke and K. Kalantar-Zadeh, *Adv. Funct. Mater.*, 2018, **28**, 1804057.

112 Y. Wang, M. Mayyas, J. Yang, M. B. Ghasemian, J. Tang, M. Mousavi, J. Han, M. Ahmed, M. Baharfar, G. Mao, Y. Yao, D. Esrafilzadeh, D. Cortie and K. Kalantar-Zadeh, *ACS Appl. Mater. Interfaces*, 2021, **13**, 53181–53193.

113 S. Cai, M. B. Ghasemian, M. A. Rahim, M. Baharfar, J. Yang, J. Tang, K. Kalantar-Zadeh and F.-M. Allioux, *Nanoscale*, 2023, **15**, 4291–4300.

114 M. Mousavi, M. B. Ghasemian, J. Han, Y. Wang, R. Abbasi, J. Yang, J. Tang, S. A. Idrus-Saidi, X. Guan, M. J. Christoe, S. Merhebi, C. Zhang, J. Tang, R. Jalili, T. Daeneke, T. Wu, K. Kalantar-Zadeh and M. Mayyas, *Appl. Mater. Today*, 2021, **22**, 100954.

115 B. J. Carey, J. Z. Ou, R. M. Clark, K. J. Berean, A. Zavabeti, A. S. R. Chesman, S. P. Russo, D. W. M. Lau, Z.-Q. Xu, Q. Bao, O. Kavehei, B. C. Gibson, M. D. Dickey, R. B. Kaner, T. Daeneke and K. Kalantar-Zadeh, *Nat. Commun.*, 2017, **8**, 14482.

116 X. Wang, R. Quhe, Y. Zhi, Z. Liu, Y. Huang, X. Dai, Y. Tang, Z. Wu and W. Tang, *Superlattices Microstruct.*, 2019, **125**, 330–337.

117 M. Akatsuka, Y. Kawaguchi, R. Itoh, A. Ozawa, M. Yamamoto, T. Tanabe and T. Yoshida, *Appl. Catal., B*, 2020, **262**, 118247.

118 X. Tang, X. Huang, Y. Huang, Y. Gou, J. Pastore, Y. Yang, Y. Xiong, J. Qian, J. D. Brock, J. Lu, L. Xiao, H. D. Abruña and L. Zhuang, *ACS Appl. Mater. Interfaces*, 2018, **10**, 5519–5526.

119 G. Litrico, P. Proulx, J.-B. Gouriet and P. Rambaud, *Adv. Powder Technol.*, 2015, **26**, 1–7.

120 M. Wang, Z. Lai, X. Jin, T. Sun, H. Liu and H. Qi, *Adv. Funct. Mater.*, 2021, **31**, 2101957.

121 M. Wang, X. Feng, X. Wang, S. Hu, C. Zhang and H. Qi, *J. Mater. Chem. A*, 2021, **9**, 24539–24547.

122 G. Shen, D. Chen, P.-C. Chen and C. Zhou, *ACS Nano*, 2009, **3**, 1115–1120.

123 P. Krempl, G. Schleinzer and W. Wallnöfer, *Sens. Actuators, A*, 1997, **61**, 361–363.

124 S. N. Mohammad, A. A. Salvador and H. Morkoc, *Proc. IEEE*, 1995, **83**, 1306–1355.

125 H. Khan, N. Mahmood, A. Zavabeti, A. Elbourne, M. A. Rahman, B. Y. Zhang, V. Krishnamurthi, P. Atkin, M. B. Ghasemian, J. Yang, G. Zheng, A. R. Ravindran, S. Walia, L. Wang, S. P. Russo, T. Daeneke, Y. Li and K. Kalantar-Zadeh, *Nat. Commun.*, 2020, **11**, 3449.

126 V. Krishnamurthi, H. Khan, T. Ahmed, A. Zavabeti, S. A. Tawfik, S. K. Jain, M. J. S. Spencer, S. Balendhran, K. B. Crozier, Z. Li, L. Fu, M. Mohiuddin, M. X. Low, B. Shabbir, A. Boes, A. Mitchell, C. F. McConville, Y. Li, K. Kalantar-Zadeh, N. Mahmood and S. Walia, *Adv. Mater.*, 2020, **32**, 2004247.

127 Q. Li, B.-D. Du, J.-Y. Gao, B.-Y. Xing, D.-K. Wang, J.-F. Ye and J. Liu, *Adv. Mater. Technol.*, 2022, **7**, 2200733.

128 N. Syed, A. Zavabeti, K. A. Messalea, E. Della Gaspera, A. Elbourne, A. Jannat, M. Mohiuddin, B. Y. Zhang, G. Zheng, L. Wang, S. P. Russo, D. Esrafilzadeh, C. F. McConville, K. Kalantar-Zadeh and T. Daeneke, *J. Am. Chem. Soc.*, 2019, **141**, 104–108.

129 Y. Du, S. Yin, Y. Li, J. Chen, D. Shi, E. Guo, H. Zhang, Z. Wang, Q. Qin and C. Zou, *Small Methods*, 2023, 2300175.

130 Y. Zhou, B. Deng, Y. Zhou, X. Ren, J. Yin, C. Jin, Z. Liu and H. Peng, *Nano Lett.*, 2016, **16**, 2103–2107.

131 Z. Chen, Q. Chen, Z. Chai, B. Wei, J. Wang, Y. Liu, Y. Shi, Z. Wang and J. Li, *Nano Res.*, 2022, **15**, 4677–4681.

132 J. Fujita, T. Hiyama, A. Hirukawa, T. Kondo, J. Nakamura, S. Ito, R. Araki, Y. Ito, M. Takeguchi and W. W. Pai, *Sci. Rep.*, 2017, **7**, 12371.

133 M. Mayyas, H. Li, P. Kumar, M. B. Ghasemian, J. Yang, Y. Wang, D. J. Lawes, J. Han, M. G. Saborio, J. Tang, R. Jalili, S. H. Lee, W. K. Seong, S. P. Russo, D. Esrafilzadeh, T. Daeneke, R. B. Kaner, R. S. Ruoff and K. Kalantar-Zadeh, *Adv. Mater. Interfaces*, 2020, **32**, 2001997.

134 S. L. James, *Chem. Soc. Rev.*, 2003, **32**, 276–288.

135 X. Hu, T. Huang, G. Zhang, S. Lin, R. Chen, L.-H. Chung and J. He, *Coord. Chem. Rev.*, 2023, **475**, 214879.

136 B. Wang, J.-H. Liu, J. Yu, J. Lv, C. Dong and J.-R. Li, *J. Hazard. Mater.*, 2020, **382**, 121018.

137 A. S. Efimova, P. V. Alekseevskiy, M. V. Timofeeva, Y. A. Kenzhebayeva, A. O. Kuleshova, I. G. Koryakina, D. I. Pavlov, T. S. Sukhikh, A. S. Potapov, S. A. Shipilovskikh, N. Li and V. A. Milichko, *Small Methods*, 2023, **7**, 2300752.

138 S. Wang, Z. Ai, X. Niu, W. Yang, R. Kang, Z. Lin, A. Waseem, L. Jiao and H.-L. Jiang, *Adv. Mater.*, 2023, **35**, 2302512.

139 R. Shu, J. Wu and X. Yang, *Composites, Part A*, 2023, **173**, 107677.

140 A. V. Parmuzina and O. V. Kravchenko, *Int. J. Hydrogen Energy*, 2008, **33**, 3073–3076.

141 J. Zheng, A. Sharma, T. Kumeria, Y. Chi, M. B. Ghasemian, G. Mao, J. Tang, P. Kumar, Md. A. Rahim and K. Kalantar-Zadeh, *Adv. Funct. Mater.*, 2023, 2300969.

142 H. Kwon, H.-N. Barad, A. R. Silva Olaya, M. Alarcón-Correa, K. Hahn, G. Richter, G. Wittstock and P. Fischer, *ACS Appl. Mater. Interfaces*, 2023, **15**, 5620–5627.

143 D. Bridges, D. Fieser, J. J. Santiago and A. Hu, *Metals*, 2023, **13**, 1193.